# Cdc123, a Cell Cycle Regulator Needed for eIF2 Assembly, Is an ATP-Grasp Protein with Unique Features

Michel Panvert, Etienne Dubiez, Lea Arnold, Javier Perez, Yves Mechulam, Wolfgang Seufert, Emmanuelle Schmitt

▶ **To cite this version:**

Michel Panvert, Etienne Dubiez, Lea Arnold, Javier Perez, Yves Mechulam, et al.. Cdc123, a Cell Cycle Regulator Needed for eIF2 Assembly, Is an ATP-Grasp Protein with Unique Features. Structure, 2015, 23 (9), pp.1596-1608. 10.1016/j.str.2015.06.014 . hal-01222821

**HAL Id: hal-01222821**

**https://hal-polytechnique.archives-ouvertes.fr/hal-01222821**

Submitted on 30 Oct 2015

**HAL** is a multi-disciplinary open access archive for the deposit and dissemination of scientific research documents, whether they are published or not. The documents may come from teaching and research institutions in France or abroad, or from public or private research centers.

L'archive ouverte pluridisciplinaire **HAL**, est destinée au dépôt et à la diffusion de documents scientifiques de niveau recherche, publiés ou non, émanant des établissements d'enseignement et de recherche français ou étrangers, des laboratoires publics ou privés.

# Cdc123, a cell cycle regulator needed for eIF2 assembly, is an ATP-grasp protein with unique features

Michel Panvert[1], Etienne Dubiez[1], Lea Arnold[2], Javier Perez[3], Yves Mechulam[1], Wolfgang Seufert*[2] and Emmanuelle Schmitt[1]*

[1]Laboratoire de Biochimie, Ecole Polytechnique, CNRS, F-91128 Palaiseau cedex, France. Phone : +33-1-69334485; Fax: +33-1-69334909

[2]Department of Genetics, University of Regensburg, D-93040 Regensburg, Germany, Phone : +49-941-943-3162; Fax: +49-941-943-3163

[3]SOLEIL Synchrotron, L'Orme des Merisiers, F-91190 Saint Aubin, France

*Co-corresponding authors: emma@bioc.polytechnique.fr and Wolfgang.Seufert@ur.de

"The authors declare that they have no conflict of interest."

Running title: Cdc123 is an ATP-grasp protein

**ABSTRACT**

Eukaryotic initiation factor 2 (eIF2), a heterotrimeric GTPase, has a central role in protein biosynthesis by supplying methionylated initiator tRNA to the ribosomal translation initiation complex and by serving as a target for translational control in response to stress. Recent work identified a novel step indispensable for eIF2 function: assembly of eIF2 from its three protein subunits by the cell proliferation protein Cdc123. We report the first crystal structure of a Cdc123 representative, that from *Schizosaccharomyces pombe*, both isolated and bound to the domain III of eIF2γ from *Saccharomyces cerevisiae*. The structures show that Cdc123 resembles enzymes of the ATP-grasp family. Indeed, Cdc123 binds ATP-$Mg^{2+}$ and conserved residues contacting ATP-$Mg^{2+}$ are essential for Cdc123 to support eIF2 assembly and cell viability. A docking of eIF2αγ onto Cdc123, combined with genetic and biochemical experiments, allows us to propose a model explaining how Cdc123 participates in the biogenesis of eIF2 through facilitating assembly of eIF2γ to eIF2α.

## INTRODUCTION

Initiation of the translation of a messenger RNA into a protein involves a complex cascade of molecular events, leading to a translation-competent ribosome with a methionylated initiator tRNA in the P-site, base-paired with the start codon on mRNA (Hinnebusch, 2011; Lorsch and Dever, 2010). A critical consequence of the whole process is the setting of the reading frame for mRNA decoding. In eukaryotic and archaeal cells, the initiator tRNA carrier is the e/aIF2 heterotrimer. e/aIF2 results from the association of three subunits, α, β and γ. The γ subunit forms the core of the heterotrimer. It interacts with both the α and the β subunits while α and β do not interact together (Schmitt et al., 2010). In its GTP-bound form, this factor specifically binds Met-tRNA$_i^{Met}$ (Schmitt et al., 2012) and handles it in the initiation complex (Huang et al., 1997). After start codon recognition, the factor, in its GDP-bound form, loses affinity for Met-tRNA$_i^{Met}$ and eventually dissociates from the initiation complex (Algire et al., 2005). This leaves Met-tRNA$_i^{Met}$ in the P site of the small ribosomal subunit and allows the final steps of initiation to occur. In this process, specific handling of the initiator tRNA by e/aIF2 and control of the nucleotide state of the factor are crucial for accuracy.

According to its central role in translation, eIF2 was early identified as a central target in response to stress conditions (Gebauer and Hentze, 2004; Holcik and Sonenberg, 2005). Such conditions trigger phosphorylation of the α subunit of the heterotrimer that, in turn, leads eIF2 to form an inactive complex with the guanine nucleotide exchange factor eIF2B. The subsequent sequestering of eIF2 reprograms gene expression by both reducing global translation and specifically enhancing the translation of mRNAs encoding activators of the transcription of stress adaptation genes (Hinnebusch, 2005).

Proteomic studies in *S. cerevisiae* have reported interaction of the γ subunit of eIF2 with the cell proliferation protein Cdc123 (*e.g* (Ho et al., 2002)). This gene was first identified in mammals as the target of mutations blocking the G1-S transition in the cell cycle (Ohno et al., 1984; Okuda and Kimura, 1996). In human, CDC123 was described as a candidate oncogene in breast cancer (Adelaide et al., 2007) and implicated in other diseases (Soler Artigas et al., 2011; Zeggini et al., 2008). Relationships between eIF2 and Cdc123 became clearer when it was shown that assembly of the eIF2

complex *in vivo* depended on Cdc123 (Perzlmaier et al., 2013). Indeed, mutations of Cdc123 in budding yeast reduced the association of the eIF2 subunits, diminished polysome levels, and increased *GCN4* expression indicating that Cdc123 was critical for eIF2 activity. Using co-immunoprecipitation from *S. cerevisiae* cell extracts as well as pull-down experiments with *E. coli* expressed proteins, an interaction between Cdc123 and the unassembled γ subunit of eIF2 was shown (Perzlmaier et al., 2013). More precisely, the results have indicated that domain III of the γ subunit of eIF2 was required for binding to Cdc123. Alterations of the binding site revealed a strict correlation between Cdc123 binding, the biological function of eIF2γ and its ability to assemble with α and β subunits. Overexpression of Cdc123 neutralized the eIF2 assembly defect. Moreover, overexpression of eIF2 α or γ subunits rescued an otherwise inviable *cdc123* deletion mutant with a strong synergistic effect when both α and γ subunits were overproduced. In contrast, overexpression of eIF2β could not compensate for the absence of Cdc123. Thus, Cdc123 has appeared as an essential protein acting as a specific assembly factor of the eIF2 heterotrimeric complex by promoting the eIF2αγ assembly step (Perzlmaier et al., 2013). The requirement of Cdc123 in eukaryotes may explain why all attempts to produce isolated yeast eIF2γ were unsuccessful (Naveau et al., 2013).

Here, we report the first crystal structure of a Cdc123 representative, that from *Schizosaccharomyces pombe,* both isolated and bound to the domain III of eIF2γ (γDIII) from *Saccharomyces cerevisiae*. Cdc123 resembles enzymes of the ATP-grasp family and indeed binds ATP-$Mg^{2+}$. Structural data and biochemical studies revealed that ATP-$Mg^{2+}$ is needed for Cdc123 activity. A docking of eIF2αγ onto Cdc123 allows us to propose a tentative model explaining how Cdc123 participates in the biogenesis of eIF2 through facilitating assembly of eIF2γ to eIF2α.

## RESULTS

*Overall structure of Sp-Cdc123*

Despite many attempts, no crystal could be obtained using Cdc123 from *S. cerevisiae* (Sc-Cdc123). Therefore, we have chosen to purify Cdc123 from *Schizosaccharomyces pombe*, Sp-Cdc123. Indeed, the two proteins share 35% identities (55% similarities). Moreover, Sp-Cdc123 is shorter than Sc-Cdc123 (319 amino acids as compared to 360 in the case of Sc-Cdc123) with smaller predicted loop regions ((Cole et al., 2008); Figure S1A). Various crystal forms of full-length Sp-Cdc123 were obtained (Table S1). The 3D structure was solved using anomalous scattering data from crystals of selenomethionylated Cdc123, combined with non-crystallographic symmetry and multi-crystal averaging. The initial density map allowed us to trace most of the Cα backbone and to identify non-crystallographic symmetry operators. This permitted partial refinement of a first 3D model of Sp-Cdc123 at 3.24 Å resolution. This model contained residues 2-271 with the exception of residues 51 to 71. The C-terminal part of the protein (272 to 319) was not visible in the electron density. We suspected that mobility of this region within the crystals might have hampered the diffraction quality. Therefore, a C-terminal truncated form of Sp-Cdc123 (1 to 274, hereafter named Sp-Cdc123Δc) was engineered. High-resolution diffracting crystals could be obtained using Sp-Cdc123Δc (Table 1). The structure was solved by molecular replacement using the 3.24 Å resolution model and refined to 2.06 Å resolution. Final statistics are given in Table 1. The final model contains two monomers of Sp-Cdc123Δc in the asymmetric unit. As in the case of the model obtained with the full-length protein, residues 51 to 71 were not defined in the electron density for both monomers and loop 148-152 was difficult to model. Notably, the C-terminally truncated protein and the full-length protein were arranged as a tetramer within the crystals. Nevertheless, Sp-Cdc123 behaved as a monomer in solution, as shown by molecular sieving and SEC-MALS (see Experimental Procedures).

The structure of Sp-Cdc123Δc monomer can be divided into two α–β domains. The N-terminal domain contains residues 2 to 170 (domain 1) and the central domain contains residues 171 to 274 (domain 2, Figure 1). A comparison of the Sp-Cdc123 structure to other known structures was performed using the Dali server (Holm and Sander, 1995). All high scoring entries in the PDB

belonged to the ATP-grasp family. Representative top scoring matches are shown figure S2B. All homologous structures shown in Figure S2B can be aligned to Cdc123 with Z-scores ranging from 8.3 to 11.2 and rmsd in the 3 Å range for 156-179 aligned residues. ATP-grasp enzymes catalyze similar reactions, involving an ATP-dependent ligation of a carboxyl group carbon with an amino or imino group nitrogen. Catalysis proceeds, in each case, through the formation of an acylphosphate intermediate (Artymiuk et al., 1996; Fan et al., 1995; Galperin and Koonin, 1997). This homology was unanticipated according to the low sequence similarities of Cdc123 with proteins of the ATP-grasp family (in the 10% range, Figure S2) and had previously not been detected using standard BLAST procedures. The classical ATP-grasp fold is formed of three domains usually named, N, central and C domains (or A, B and C (Fawaz et al., 2011). The N domains are not structurally conserved between the various ATP-grasp enzymes. Comparison of ATP-grasp enzymes with Cdc123 (Figures 2 and S2) shows, however, that the structural homology is restricted to the central and C domains (equivalent to domains 1 and 2 in Cdc123, respectively; Figure 2C). Indeed, the N terminal domain of ATP-grasp enzymes (colored gray in Figure S2B) is not observed in Cdc123 proteins. Domain 1 of Cdc123 contains a three-stranded β-sheet, whereas the corresponding β-sheet in ATP-grasp enzymes contains a fourth strand (Figure 2B). Residues forming this additional strand are inserted between β2 and β3 counterparts of Cdc123 domain 1 (Figure S2A). Domain 2 of Cdc123 contains a four-stranded antiparallel β-sheet with a topology similar to that observed in the C-terminal domain of ATP-grasp enzymes (Figure S2). A fifth β-strand is observed at the C-terminal part of Cdc123Δc. Finally, within domains 1 and 2, regions specific to Cdc123 are inserted or divergent (colored green in Figure 2 and in Figure S2). Among these are regions involved in ATP binding in grasp enzymes (colored orange in Figures 2 and S2 (Fan et al., 1995)).

Despite these differences, the obvious resemblance of Cdc123 with ATP-grasp enzymes suggested that Cdc123 had the ability to bind ATP.

*Cdc123 binds ATP*

As an attempt to evidence ATP binding by Sp-Cdc123, a titration of the protein with ATP was followed using ITC (Experimental Procedures). A dissociation constant of 67 ± 13 µM could be deduced from the titration curve (Figure S3). This Kd value is in the same range as that measured for a typical ATP-grasp enzyme, the *S. aureus* D-alanine:D-alanine ligase (60µM, Liu et al ., 2006). This result shows that Sp-Cdc123 indeed binds ATP with significant affinity.

In order to obtain further insight into ATP binding, crystallization trials with Sp-Cdc123Δc were performed in the presence of ATP-$Mg^{2+}$, AMP-PNP-$Mg^{2+}$ and ADP-$Mg^{2+}$. Crystals isomorphic to crystals with unliganded Sp-Cdc123Δc were obtained and datasets were collected. However, a bound nucleotide was only observed when crystals were prepared in the presence of AMP-PNP. In this case, there was no density for the γ-phosphate group in the maps and therefore the density was assigned to an ADP molecule. Instability of AMP-PNP in acidic conditions has been reported (Sigma-Aldrich product information sheet) and could explain the presence of ADP instead of AMP-PNP. Only one ADP molecule bound to monomer A was clearly identified (Table 1, Figure 3). No magnesium ion bound to ADP was observed. In monomer B, residual electron density within the pocket was attributed to water molecules. Their positions may reflect low occupancy of ADP. Possibly, packing constraints may have hampered tight binding of ADP to the second monomer.

In monomer A, ADP is bound in a position corresponding to the ATP binding pocket previously identified in ATP-grasp enzymes, at the interface between the domain 1 and domain 2 (Figures 1 and 2). One side of the ADP molecule is held by residues located in domain 2 of Cdc123, belonging to motifs conserved in all ATP-grasp enzymes (yellow residues in β4-β7, Figure 3A). At the opposite side, some residues belonging to domain 1 participate in the binding of ADP (residues 164-167, blue residues in Figure 3A). Additional contacts involve residues located in non-conserved regions (residues 99, 101, 103, colored green in Figure 3A). Interestingly, the two regions corresponding to the loops involved in ATP binding in ATP-grasp enzymes, named “small loop” and “large loop” (Figure 2B and S2, residues 176-180 and 233-261 in 1E4E), are highly divergent in Cdc123. These two regions of ATP-grasp enzymes form a lid in the presence of ATP, interacting together above the ATP binding cavity (Figure 2B and S2 (Fan et al., 1995; Hara et al., 1996; Roper et al., 2000; Zhao et al., 2013)). In place of the small loop segment, region 98-110 contains stretches of

residues highly conserved in Cdc123 proteins (Figure S1). Finally, comparison of the structure of unliganded Cdc123 with that of ADP-bound Cdc123 only showed adjustments of side chains involved in the binding of ADP.

Overall, analysis of the ADP binding site in Cdc123 shows that nucleotide binding involves regions and residues of the protein that are conserved in ATP-grasp enzymes (Figure S2). This observation makes a strong case for a common ancestry of Cdc123 and ATP-grasp enzymes. However, significant differences are observed within their respective ATP binding sites. Such divergences are likely to be linked to the biological function of Cdc123. Overall, Cdc123 may be considered as an atypical member of the ATP-grasp family.

Notably, a second cavity faces the nucleotide-binding pocket in Cdc123 (Figure 3B). This cavity is walled by residues V10, C13 and Q14 from α1 on one side and by residues H134, D135 and F140 from α6 on the other side. In addition, the side chains of R246 and W99 are positioned at the top and bottom of the cavity, respectively. In the ADP-bound structure, the cavity is filled up by electron density attributed to five water molecules. According to the location of the second binding pocket and to the homology with the ATP-grasp enzymes, it is conceivable that this pocket corresponds to a binding site for a second ligand of Cdc123, substrate of a reaction involving an ATP-dependent ligation step as observed in ATP-grasp enzymes. The existence of such an unidentified second ligand remains however hypothetic at this stage.

*Binding of Cdc123 to eIF2γ*

*In vivo* assembly of the eIF2 complex was shown to depend on Cdc123. Sc-Cdc123 activity involved an interaction with the unassembled eIF2γ subunit (Perzlmaier et al., 2013). eIF2γ is made of three domains: the GTP-binding domain, γDI, and the two β-barrels γDII and γDIII (Schmitt et al., 2010). Within eIF2γ, domain III was shown to be sufficient for binding to Cdc123 (Perzlmaier et al., 2013).

According to these results, we evidenced *in vitro* interaction of Sc-Cdc123 to Sc-eIF2γDIII domain (domain III of eIF2γ from *S. cerevisiae*) using molecular sieving experiments (Figure S3 and

Experimental Procedures). Interestingly, the behavior of Sc-Cdc123 on the molecular sieve column suggested that the protein was dimeric in its unliganded form and became monomeric upon binding to eIF2γDIII (Figure S3). The Kd value for the binding of Sc-eIF2γDIII to Sc-Cdc123 was 2.5 ± 0.5 µM, as measured using ITC (Figure S3). This value was measured in the absence of ATP. Hence, binding of Sc-eIF2γDIII to Sc-Cdc123 did not strictly require the presence of ATP-$Mg^{2+}$. Despite several attempts, no crystal could be obtained using the purified complex. Therefore, we decided to design a chimeric complex made of Sp-Cdc123 bound to Sc-eIF2γDIII. Formation of a stable complex was indeed observed by a pull-down experiment showing that an N-terminally his-tagged version of Sp-Cdc123 can trap Sc-eIF2γDIII on a cobalt affinity resin. Upon elution with imidazole, a peak corresponding to a heterodimer of Sp-Cdc123 bound to Sc-eIF2γDIII was observed (Experimental Procedures). An additional step using molecular sieving allowed us to polish the purification (Figure S3). Notably, the binding of Sc-eIF2γDIII to Sp-Cdc123 did not produce sufficient heat changes to allow accurate determination of a Kd value using ITC. One possible explanation is that, in the case of the complex formed with the *S. cerevisiae* proteins, binding of Sc-Cdc123 to Sc-eIF2γDIII is accompanied by a change of the oligomeric state of Sc-Cdc123 from homodimer to monomer. Sp-Cdc123 behaves as a monomer and binding to Sc-γDIII does not change its oligomeric state, possibly explaining why observed heat changes are weaker.

Suitable crystals were obtained using the purified complex Sp-Cdc123:Sc-eIF2γDIII at 24°C in the presence or in the absence of ATP-$Mg^{2+}$. The structure was solved by molecular replacement using the structure of Sp-Cdc123Δc determined in this study and the structure of aIF2γDIII from *S. solfataricus* (2AHO, (Yatime et al., 2006)) as search models. The structures were refined to 2.9 Å and 3.0 Å resolution in the presence or in the absence of ATP-$Mg^{2+}$, respectively (Table 1).

Within the complex, the structure of the γDIII domain was defined from residue 423 to residue 524 with only the 3 C-terminal residues not visible in the electron density. In Sp-Cdc123, all residues corresponding to the two core domains (from 2 to 274) were visible with the exception of two loops (residues 53 to 68 and residues 149 to 152). Residues 275 to 296 were not visible. However, additional electron density disconnected from the main structure was attributed to a long helix of the C-terminal

domain of Sp-Cdc123 (α10, residues 297 to 315). Superimposition of the structure of the complex obtained in the presence of ATP on that obtained without ATP showed only adjustments of side chains involved in the binding of ATP.

*Overall structure of Sp-Cdc123:Sc-eIF2γDIII*

Sc-eIF2γDIII forms a β-barrel highly homologous to the corresponding domain in archaeal aIF2 (Figure S4). Two differences are notable. In the eukaryotic domain, (i) the loop between β16 and β17 is longer and, (ii) β21 is extended by four residues in such a way that its interaction with strand β16 is reinforced.

In the structure of the complex, the γDIII domain is bound to one side of Cdc123 domain 1. Neither Cdc123-domain 2 nor the C-terminal helix α10 does contact γDIII (Figure 4A). γDIII and Cdc123 closely interact together with an interaction surface of 1307 $Å^2$. Interestingly, the binding site of γDIII to Cdc123 overlaps the dimerization site of Cdc123 observed in all crystal forms. In order to address the possibility that the observed position of γDIII to Cdc123 may have resulted from crystallization artifacts, a solution study was carried out using small angle X-ray scattering. The goal was to compare theoretical X-ray scattering curve deduced from the crystallographic structure with the scattering curve experimentally observed in solution. As shown in Figure 4B, the SAXS experimental curve obtained with the purified Sp-Cdc123:Sc-eIF2γDIII fits very nicely the curve calculated from the crystal structure coordinates. This strongly argues in favor of the biological significance of our crystalline model.

Detailed interactions of Sp-Cdc123 with Sc-eIF2γDIII are shown in Figure 4C and D. Sc-eIF2γDIII is mainly bound through its concave side formed by strands β17-β18-β19-β20-β21 of the barrel and by the β20-β21 loop (Figure 4D). On the side of Cdc123, the main regions of contacts correspond to α3 and the following loop (residues 44, 46-50), helix η2 (residues 107-110), α5 and α6 (Figure 4C). Notably, the Cdc123 regions involved in the binding of Sc-eIF2γDIII correspond to regions specific of Cdc123 proteins, not found in ATP-grasp enzymes (Figures 2 and S2, green regions). Figures S1, S4 and Table 2 show residues involved in the heterodimer interface between

Cdc123 and γDIII. Superimposition of bound Cdc123 on unbound Cdc123 showed that binding to γDIII involved adjustment of the interface regions. In particular, α3 and the following loop are displaced and the conformation of the region around helix η2 (residues 107-110) is adjusted. This part of Cdc123 is connected to the ATP binding pocket (Figure 4C and D). Nevertheless, the Kd value of ATP measured by ITC for Sp-Cdc123:Sc-eIF2γDIII (57 ± 7 μM ) was not significantly changed as compared to that measured for isolated Sp-Cdc123 (67 ± 13 μM).

Previous results had suggested that within domain III, the C-terminal tail, specific of eukaryotic eIF2γ was required for the interaction with Cdc123. Indeed, removal of thirteen amino acids at the C-terminal extremity of eIF2γ (residues 515 to 527) was sufficient to render the protein non-functional in the binding to Cdc123 or to eIF2α and eIF2β subunits (Perzlmaier et al., 2013). On the contrary, the removal of 4 amino acids from the C-terminus was tolerated, since binding to Cdc123 and assembly with α and γ subunit still occurred (Perzlmaier et al., 2013). No direct interaction is observed between the C-terminal part of γDIII and Cdc123 in the structure of the complex. However, the structure shows that the last β-strand of γDIII (β21) is extended to residue 522. Therefore, it is likely that a deletion of residues belonging to β21 led to destabilization of the structure of the β-barrel and thereby impaired binding to Cdc123. According to these observations, the absence of C-terminal extension in archaeal aIF2γDIII cannot be straightforwardly related to the absence of Cdc123 from archaea.

To further characterize the complex between Cdc123 and eIF2γDIII, mutations within γDIII were introduced. Three single mutants were produced, E460A, R504A and W509A. The effect of the mutations on association with Sp-Cdc123 was evaluated using pull-down assays (Figure S4). As predicted from the 3D structure, modification of R504 and W509 into alanine resulted in lower amount of Sp-Cdc123:Sc-eIF2γDIII complex retained on affinity column, as compared to that obtained with wild-type Sc-eIF2γDIII (Figure S4). In the case of E460A mutant, a lower level of protein expression did not allow us to reach a firm conclusion.

*ATP binding residues of Cdc123 are crucial for eIF2 assembly*

Crystals of Sp-Cdc123:Sc-eIF2γDIII complex could be obtained in the presence of ATP-$Mg^{2+}$ (Table 1). As shown in Figures 5 and S5A, ATP-$Mg^{2+}$ is observed, firmly bound to Cdc123 in the presence of one $Mg^{2+}$ ion. The octahedral coordination of the tightly bound magnesium ion is visible. In the equatorial plane, four bonds involve D239 and N241 side chains and two oxygens from the β and γ phosphate groups. Two water molecules are in apical positions. One of them is stabilized by D227, whereas the second water appears less stable. Superimposition of Sp-Cdc123:Sc-eIF2γDIII:ATP on Cdc123Δc:ADP shows that the two structures are nearly identical in the area of the nucleotide, with only adjustments of side chain residues involved in the binding of $Mg^{2+}$ and of the γ phosphate group (Figure S5B).

Interestingly, in-line with the γ-phosphate of ATP is a water molecule located at 3.3 Å from the oxygens, at the entrance of the second cavity. This water molecule, stabilized by interactions with the main chain NH group of D248 and with the side chain $NH_2$ group of R176, would be correctly positioned to participate in a possible ATP hydrolysis reaction (Figure 5A and Figure S5B). At this moment, however, such an activity has not been firmly established.

To get further insight into the role of ATP in eIF2 assembly, mutants of Sc-Cdc123 were designed and their behaviors were studied *in vivo*.

We targeted residues involved in the coordination of the ATP-bound $Mg^{2+}$ ion. Indeed, these residues (D227, D239, N241 in Sp-Cdc123) are highly conserved in Cdc123 sequences and in ATP-grasp enzymes (Figures S1 and S2). Moreover, various studies of ATP-grasp enzymes have shown that these residues are essential for the enzymatic activity and suggested that $Mg^{2+}$ had a catalytic role by maintaining ATP into a correct conformation for catalysis (Miller et al., 2005; Sloane et al., 2001). Therefore, we mutated the "DIN" sequence of Sc-Cdc123 (DIN; 266-268 in Sc-Cdc123 corresponding to 239-241 in Sp-Cdc123, Figure S1) into three alanines. To test the effect of the DIN mutation *in vivo,* we used diploid yeast cells heterozygote for a *CDC123* gene deletion, and expressing either wild type *CDC123* or the DIN mutant (Figure 5B, right panel). No complementation of a deletion of the *CDC123* gene was observed in the presence of the Sc-Cdc123 DIN. Moreover, the DIN mutant also failed to support assembly of Sc-eIF2γ with eIF2α (Figure 5B, left panel). This observation was made

in a *S. cerevisiae* strain deleted for *CDC123* and kept alive by high-level expression of eIF2γ and eIF2α. Relative to a strain that carries the *CDC123* gene, there was much less eIF2γ-eIF2α association in the *cdc123* deletion mutant. Expression of the wild type version of Cdc123 restored normal eIF2γ-eIF2α association. Expression of the Sc-Cdc123 DIN mutant, however, failed to increase the association of eIF2γ with eIF2α (Figure 5B, left panel). Thus, ATP-binding residues are essential for Cdc123 to support cell viability and eIF2γ-eIF2α assembly. Using co-IP experiments, we observed a defect of the DIN mutant in its interaction with full-length eIF2γ, whereas the amount of co-precipitated eIF2α was unaffected by the DIN mutation (Figure S6A). This points to a link between ATP and the binding of full-length eIF2γ by Cdc123.

To substantiate these observations, we analyzed another mutant of the ATP binding site of Cdc123, Sc-CDC123-D252A (equivalent to *S. pombe* D227) mutant. This residue, as D266 and N268, participates in the binding of the magnesium ion through a water-mediated interaction (Table 3). In line with the DIN mutant, Sc-CDC123-D252A failed to complement a *CDC123* gene deletion and did not support assembly of eIF2γ with eIF2α (Figure 5B). Together, these data show that the DIN and D252A mutations disrupt both the biological and biochemical function of Cdc123. Hence, these results strongly argue in favor of a requirement on ATP binding for the vital cellular function of Cdc123 and for its role in promoting eIF2αγ assembly.

*Model for the catalytic complex*

In order to go forward in understanding the mechanism used by Cdc123 for eIF2 assembly, we performed a docking model for the binding of eIF2γ onto Cdc123. According to structural alignments and biochemical data, the 3D structure of the eukaryotic γ subunit is supposed to be very close to that of its archaeal counterpart (Schmitt et al., 2012). Therefore, to make the docking model, the Sc-eIF2γDIII domain from the Sp-Cdc123:γDIII structure, was superimposed on the corresponding domain in aIF2γ structure (4RD4, (Dubiez et al., 2015)). In this model, shown in Figure 6A and B, the complete eIF2γ subunit is nicely anchored to Cdc123, without intertwining. Interestingly, the docking model revealed another potential contact between eIF2γ and Cdc123. This contact would involve the

long L1 loop of aIF2γ-DII domain and the loop linking β5 to α7 (residues 192-196) of Sp-Cdc123. Strikingly, L1 loop of e/aIF2γ-DII domain is known to mediate interaction between e/aIF2γ and e/aIF2α subunits (Naveau et al., 2013; Roll-Mecak et al., 2004; Schmitt et al., 2002; Yatime et al., 2006).

Importantly, the position of eIF2γ on Cdc123 is compatible with simultaneous binding to eIF2α. Indeed, the docking model can be completed by positioning the aIF2α subunit, thanks to the knowledge of the aIF2αγ structure (PDB ID Code 2AHO, (Yatime et al., 2006)). As shown in Figure 6C, the model suggests an interaction of Cdc123 with the interface between α and γ subunits. Hence, the docking model opens the possibility that Cdc123 acts through transient interaction with the L1 loop of γDII and domain 3 of eIF2α subunit. This interaction would be necessary for the assembly of eIF2γ and eIF2α.

To test the docking model, we generated a mutant version of eIF2γ lacking part of the L1 loop and analyzed its interaction with Sc-Cdc123 and the α and β subunits in an Y2H assay. The L1 loop mutation had little or no effect on the interaction of eIF2γ with eIF2β, but disrupted the interaction of eIF2γ with eIF2α and reduced the interaction of eIF2γ with Cdc123 (Figure S6B). The Y2H data, therefore, confirm the L1 loop region as an α-γ binding site in eukaryotic eIF2 orthologs and support the notion of a physical contact between the L1 loop of eIF2γ and Cdc123, as predicted by the docking model.

To further analyze the docking model, we asked for an interaction of Sc-Cdc123 with eIF2α. To this end, we over-expressed a flag3-tagged version of Sc-Cdc123 in a yeast strain whose endogenous eIF2α-encoding gene was fused to a myc13-tag. Indeed, eIF2α-myc13 was detected in anti-flag immunoprecipitates of Cdc123. This signal was specific, because it was absent from precipitates of a control strain, which lacked Cdc123-flag3 but expressed eIF2α-myc13 (Figure S6A). This experiment demonstrates a contact between Cdc123 and eIF2α or eIF2αγ. Compared to the relative amount of eIF2γ co-precipitated with Cdc123-flag3 from cell extracts, much lower levels of eIF2α-myc13 were recovered. The Cdc123- eIF2α or -eIF2αγ contact might therefore be transient.

## DISCUSSION

The present study revealed the 3D structure of the cell proliferation protein Cdc123. This protein resembles enzymes belonging to the ATP-grasp superfamily. As suggested by this resemblance, ATP binding to Cdc123 could indeed be evidenced using biochemical tools and 3D structure determination. ATP is bound by residues common to Cdc123 and ATP-grasp enzymes but also by residues specific to Cdc123. Moreover, ATP-grasp enzymes possess an N-terminal domain, which makes part of their catalytic center. This domain is absent in Cdc123. Overall, Cdc123 protein appears as a member of the ATP-grasp family having unique features.

As in ATP-grasp enzymes, crucial residues are involved in the binding of the magnesium ion held on ATP. These residues (D252, D266, N268 in Sc-Cdc123 equivalent to D227, D239, N241 in Sp-Cdc123) were shown in this study to be essential for the cellular function of Cdc123. In the same view, it should be reminded that a temperature-sensitive mutant of a rat fibroblast line, arrested in the G1 phase of the cell cycle at restrictive temperature, was mapped within Cdc123 (Ohno et al., 1984; Okuda and Kimura, 1996). The mutation identified corresponds to a change of A109 into valine (equivalent to T101 in Sp-Cdc123). T101 indeed participates in the binding of ATP (Table 3). Therefore, this temperature-sensitive mutant gives further credit to the idea that ATP is needed for the cellular function of Cdc123.

Previous studies had shown that Cdc123 was necessary for eIF2 assembly (Perzlmaier et al., 2013). In particular, interaction between unassembled eIF2γ and Cdc123 was evidenced, with DIII domain of eIF2γ being sufficient to trap Cdc123. Here, we determined the structure of Sp-Cdc123 bound to the γDIII domain of eIF2. The γDIII domain of eIF2 is bound to Cdc123 via interactions involving only Cdc123-domain 1. Domain 2 and the C-terminal domain do not contact γDIII. This observation is consistent with results obtained using a yeast-2-hybrid assay and immunoprecipitation experiments, showing that C-terminal sequences of Sc-Cdc123 are dispensable for γ binding (Figure S6C). On the contrary, this C-terminal region is essential for Cdc123 function because cells carrying Cdc123Δ291 are inviable (Figure S6C). Consistently, association of the eIF2 subunits was

compromised when a truncated version of Sc-Cdc123 (Sc-Cdc123Δ327) was used (Perzlmaier et al., 2013).

Accordingly, the docking model suggests that the C-terminal domain of Cdc123 is involved in the assembly process of eIF2γ to eIF2α. Therefore, eIF2γ would be bound to Cdc123 by an anchoring point located in domain 1 of the Cdc123, as observed in the present Cdc123-γDIII structure. In this view, the Cdc123-γDIII structure might represent a "pre-assembly complex" (Figure 6). A second contact point, possibly dependent on ATP binding and/or ATP hydrolysis, involving domain 2 and the C-terminal domain of Cdc123 would be necessary for the reshaping of the interaction surface between eIF2γ and eIF2α. Once assembled, the eIF2αγ complex becomes stably folded allowing further spontaneous binding of the eIF2β subunit without the help of Cdc123 ((Perzlmaier et al., 2013) and our unpublished observations). After assembly, Cdc123 no longer interacts with eIF2 (Perzlmaier et al., 2013) even though the region of γDIII involved in Cdc123 interface remains accessible (Figure 6C). This suggests that the release of Cdc123 might result from unfavourable interactions between the second contact point (domain 2 and C-terminal domain of Cdc123) and the reshaped eIF2αγ association surface.

Notably, archaea do not display Cdc123 orthologs. Accordingly, assembly of aIF2 subunits occurs spontaneously *in vitro* (Pedulla et al., 2005; Stolboushkina et al., 2008; Yatime et al., 2006; Yatime et al., 2004). However, Sequence alignments highlighting the specificities of eukaryotic and archaeal e/aIF2γ do not give any obvious clue to explain the different behaviors of eIF2 and aIF2 regarding the assembly of the heterotrimer (Yatime et al., 2007).

Affecting ATP binding to Cdc123 led to the loss of Cdc123 function. Thus, our structural and biochemical data link the function of Cdc123 in eIF2 assembly to the cell energetics. This reinforces the idea that Cdc123 is an important control point of the eukaryotic cell cycle. The question of whether Cdc123 uses ATP in a chaperone-like fashion to support eIF2αγ assembly without covalent modification or whether Cdc123 uses ATP to introduce a post-translational modification in an effector site remains open. The existence of a second binding pocket identified in the structure rather argues in favor of the second possibility. However, for the while, our attempts to evidence modification in

purified eIF2γ subunit from cells expressing or not Cdc123 have been fruitless. Therefore, further studies are clearly required to reveal how Cdc123 uses ATP to favor the assembly of eIF2.

## EXPERIMENTAL PROCEDURES

### Protein expression and purification

*Sp-Cdc123*

The gene coding for Sp-Cdc123 was amplified from a cDNA library (generous gift from François Lacroute, INRA, Grignon, France) and cloned into pET3a and pET15b derivatives. The resulting plasmids called pET3a-SpCdc123 and pET15b-SpCdc123 led to the expression of an untagged and an N-terminally tagged version of Sp-Cdc123, respectively. To express the protein, the desired plasmid was transformed into *E. coli* BL21 Rosetta pLacI-Rare (Merck, Novagen). 1 L cultures were in 2xTY containing 50 µg/mL of ampicillin and 34 µg/mL of chloramphenicol. Expression was induced by adding 1 mM of IPTG in an overnight 37°C culture. After induction, the cultures were continued for 5 hours at 18°C.

For untagged Sp-Cdc123, cells corresponding to 1 L of culture were disrupted by sonication in 30 mL of buffer A (10 mM HEPES pH 7.5, 200 mM NaCl, 3 mM 2-mercaptoethanol, 0.1 mM PMSF, 0.1 mM benzamidine). The crude extract was loaded onto a Q-Sepharose column (16 mm x 20 cm; GE-Healthcare) equilibrated in buffer A. A gradient from 200 mM NaCl to 1 M NaCl was used for elution (200 mL at a flow rate of 2.5 mL/min). This step was repeated twice. The recovered protein was loaded onto a Superdex 200 10/300 (GE-Healthcare) equilibrated in buffer A. The Sp-Cdc123 pool was concentrated to 10 mg/mL. Sp-Cdc123 behaves as a monomer in solution, as shown by conventional size-exclusion chromatography coupled to multi-angle static light scattering (SEC-MALS, Wyatt).

A truncated version of Sp-Cdc123 was engineered by introducing a stop codon in place of codon 275. The obtained plasmid, pET15b-SpCdc123Δc produced a protein ending at residue 274 and carrying a poly histidine tag at the N-terminal extremity. pET15b-SpCdc123Δc was transformed into *E. coli* BL21 Rosetta and expression was obtained as described above. After sonication, the crude extract was loaded onto a column (4 mL) containing Talon affinity resin (Clontech) equilibrated in buffer B (10 mM HEPES pH 7.5, 500 mM NaCl, 3 mM 2-mercaptoethanol, 0.1 mM PMSF, 0.1 mM benzamidine). The protein was eluted with buffer B containing 125 mM imidazole. The recovered

protein was then loaded onto a Superdex 200 column (10/300; GE Healthcare) equilibrated in buffer B. The Sp-Cdc123Δc pool was concentrated to 10 mg/mL.

*Sp-Cdc123:Sc-γDIII complex*

The gene coding for the γDIII domain (fragment 410-527) of Sc-eIF2 from PWS3915 (Perzlmaier et al., 2013) was cloned in pET3alpa. The obtained plasmid pET3a-Sc-γDIII was transformed into *E. coli* BL21 Rosetta and expression was obtained as described above.

To purify the Sp-Cdc123:Sc-γDIII complex, pellets corresponding to 1 liter of culture of BL21 Rosetta *E. coli* cells transformed with pET3a-Sc-γDIII and to 1 liter of culture of BL21 rosetta *E. coli* cells transformed with pET15b-Sp-Cdc123 were resuspended in buffer B (10 mM HEPES pH 7.5, 500 mM NaCl, 3 mM 2-mercaptoethanol, 0.1 mM PMSF, 0.1 mM benzamidine) and mixed. After sonication, the crude extract was loaded onto a column (4 mL) containing Talon affinity resin (Clontech) equilibrated in buffer B. Finally, the protein complex was eluted with buffer B containing 125 mM imidazole. The recovered protein complex was finally loaded onto a Superdex 200 column (10/300; GE Healthcare) equilibrated in buffer B. Fractions containing Sp-Cdc123:Sc-γDIII were pooled and concentrated to 10 mg/mL (Figure S3B).

**Crystallization and structure determinations**

*Sp-Cdc123*

Initial crystallization trials were performed at 4°C and 24°C using sitting drops made with a Mosquito robot (TTP Labtech) and standard commercial kits (Hampton Research and Qiagen). Crystals were rapidly obtained using full-length Cdc123 in the presence of PEG3350 as precipitating agent at 24°C (see detailed conditions in Table S1). Diffraction data were collected at 100 K (λ=0.984 Å) on the Proxima-1 beamline at the SOLEIL synchrotron (Saint-Aubin, FRANCE) equipped with a Pilatus detector. Data corresponding to crystals belonging to various space groups were collected (Table S1). These crystals diffracted to a maximum of 3.0 Å resolution. Diffraction images were

analyzed with XDS (Kabsch, 1988), and the data were processed with programs of the CCP4 package (Collaborative computational project No.4, 1994).

Crystals were also obtained using the selenomethionylated version of full-length Cdc123. Highly redundant anomalous datasets were collected at 100K at a wavelength corresponding to the maximal absorption of selenium (λ=0.9792 Å). According to the weak diffraction pattern and to the modest resolution limit of diffraction (around 4 Å), two datasets collected from Se-met crystals grown in the same drop, were merged. A first experimental map was calculated at 5.5 Å resolution using the automated SAD phasing procedure of the Solve program within the Phenix suite (Adams et al., 2010). A first round of automatic building was performed within this map using the "Phase and Build" function in Solve. The partial model allowed determination of the non-crystallographic symmetry operators. In a second step, a dataset corresponding to a crystal of full-length Cdc123 obtained in space group $P2_12_12_1$ was used to perform multiple crystal averaging (Table S1). The quality of the resulting map was clearly improved and allowed manual building of a first model in Coot (Emsley et al., 2010). During manual building, the Dali Server was used to search for possible homologous structures. The crystal structure of the D-alanine--D-Alanine Ligase from *Bacillus anthracis* complexed with ATP (PDB ID code 3R5X) was identified and then used as a guide to facilitate further model building. In the course of refinement, the dataset corresponding to a crystal belonging to space group C222 was finally used to complete building of the model (Table S1). The preliminary structure of Cdc123 was partially refined to 3.24 Å resolution (R=0.2689, Rfree=0.3079). This first model revealed that full-length Cdc123 was only partly defined in the electron density with residues 274 to 319 being not visible. Therefore, in order to improve the quality of the crystals, a C-terminally truncated form of Cdc123 was then engineered. Crystals obtained with the C-terminally truncated form of Cdc123 (Sp-Cdc123Δc) diffracted to 1.85 Å resolution (see detailed conditions in Table 1). New datasets were collected in the presence or in the absence of ATP or ATP analogs (Table 1). The 3.24 Å resolution model was used to solve the structures by molecular replacement using Phaser. The final structures of Cdc123Δc were refined to 1.85 Å and 2.06 Å resolution, in the presence or in the absence of ADP, respectively, using standard procedures in Phenix. Final statistics are shown in Table 1.

*Sp-Cdc123:Sc-eIF2γDIII* complex

The complex stored in buffer B was used for crystallization trials. Crystals were obtained in the presence of 25% PEG3350 and 0.2 M $LiSO_4$ with or without ATP-$Mg^{2+}$ (see detailed conditions in Table 1). Datasets were collected on the PX1 beamline at the SOLEIL synchrotron (Saint-Aubin, FRANCE). The same procedure as the one described above was used to process the data. The structure was solved by molecular replacement with Phaser (Storoni et al., 2004), using the Cdc123Δc structure determined in this work and the γDIII domain from archaeal aIF2γ (PDB ID code 2AHO) as search models. The final structures were refined to 2.9 Å and 3.0 Å resolution in the presence or in the absence of ATP-$Mg^{2+}$, respectively (Table 1). According to the relatively modest resolution of the dataset as well as to the high B value of the structure, attribution of the sequence in the disconnected helix 275-296 remained tentative.

**Accession numbers**

Structure coordinates, 4ZGO (Sp-Cdc123Δc), 4ZGP(Sp-Cdc123Δc:ADP), 4ZGN (Sp-Cdc123:Sc-γDIII:ATP), 4ZGQ (Sp-Cdc123:Sc-γDIII) have been deposited to the PDB.

## AUTHOR CONTRIBUTIONS

ES, WS, YM designed research. MP, ED, LA, JP, ES, YM performed the experiments. ES, WS, YM wrote the paper and all authors revised the manuscript.

## ACKNOWLEDGEMENTS

This work was supported by grants from the Centre National de la Recherche Scientifique and by Ecole polytechnique to Unité Mixte de Recherche n°7654. ED was a recipient of a Gaspard Monge PhD fellowship from Ecole polytechnique. We thank the staff of the macromolecular crystallography beamlines at the SOLEIL synchrotron (Saclay, France) and in particular Pierre Legrand, for expert assistance during data collection and Andrea Brücher, Antje Machetanz-Morokane, and Adelheid Weissgerber for their expert technical assistance with the yeast work. We thank François Lacroute (Institut National de la Recherche Agronomique, Grignon, France) for generous gift of the *S. pombe* cDNA library.

## REFERENCES

Adams, P.D., Afonine, P.V., Bunkóczi, G., Chen, V.B., Davis, I.W., Echols, N., Headd, J.J., Hung, L.-W., Kapral, G.J., Grosse-Kunstleve, R.W.*, et al.* (2010). PHENIX: a comprehensive Python-based system for macromolecular structure solution. Acta Cryst *D66*, 213-221.

Adelaide, J., Finetti, P., Bekhouche, I., Repellini, L., Geneix, J., Sircoulomb, F., Charafe-Jauffret, E., Cervera, N., Desplans, J., Parzy, D.*, et al.* (2007). Integrated profiling of basal and luminal breast cancers. Cancer research *67*, 11565-11575.

Algire, M.A., Maag, D., and Lorsch, J.R. (2005). Pi release from eIF2, not GTP hydrolysis, is the step controlled by start-site selection during eukaryotic translation initiation. Mol Cell *20*, 251-262.

Artymiuk, P.J., Poirrette, A.R., Rice, D.W., and Willett, P. (1996). Biotin carboxylase comes into the fold. Nat Struct Biol *3*, 128-132.

Cole, C., Barber, J., and Barton, G. (2008). The Jpred 3 secondary structure prediction server. Nucleic Acids Research *35 (suppl.2)*, W197-W201.

Collaborative computational project No.4 (1994). The CCP4 suite: programs from protein crystallography. Acta Cristallogr *D50*, 760-763.

Dubiez, E., Aleksandrov, A., Lazennec-Schurdevin, C., Mechulam, Y., and Schmitt, E. (2015). Identification of a second GTP-bound magnesium ion in archaeal initiation factor 2. Nucleic Acids Res *43*, 2946-2957.

Emsley, P., Lohkamp, B., Scott, W.G., and Cowtan, K. (2010). Features and development of Coot. Acta Crystallogr *D66*, 486-501.

Fan, C., Moews, P.C., Shi, Y., Walsh, C.T., and Knox, J.R. (1995). A common fold for peptide synthetases cleaving ATP to ADP: glutathione synthetase and D-alanine:d-alanine ligase of Escherichia coli. Proc Natl Acad Sci U S A *92*, 1172-1176.

Fawaz, M.V., Topper, M.E., and Firestine, S.M. (2011). The ATP-grasp enzymes. Bioorg Chem *39*, 185-191.
Galperin, M.Y., and Koonin, E.V. (1997). A diverse superfamily of enzymes with ATP-dependent carboxylate-amine/thiol ligase activity. Protein Sci *6*, 2639-2643.
Gebauer, F., and Hentze, M.W. (2004). Molecular mechanisms of translational control. Nat Rev Mol Cell Biol *5*, 827-835.
Hara, T., Kato, H., Katsube, Y., and Oda, J. (1996). A pseudo-michaelis quaternary complex in the reverse reaction of a ligase: structure of Escherichia coli B glutathione synthetase complexed with ADP, glutathione, and sulfate at 2.0 A resolution. Biochemistry *35*, 11967-11974.
Hinnebusch, A.G. (2005). Translational regulation of GCN4 and the general amino acid control of yeast. Annual review of microbiology *59*, 407-450.
Hinnebusch, A.G. (2011). Molecular mechanism of scanning and start codon selection in eukaryotes. Microbiol Mol Biol Rev *75*, 434-467.
Ho, Y., Gruhler, A., Heilbut, A., Bader, G.D., Moore, L., Adams, S.L., Millar, A., Taylor, P., Bennett, K., Boutilier, K.*, et al.* (2002). Systematic identification of protein complexes in Saccharomyces cerevisiae by mass spectrometry. Nature *415*, 180-183.
Holcik, M., and Sonenberg, N. (2005). Translational control in stress and apoptosis. Nat Rev Mol Cell Biol *6*, 318-327.
Holm, L., and Sander, C. (1995). Dali: a network tool for protein structure comparison. Trends Biochem Sci *20*, 478-480.
Huang, H.K., Yoon, H., Hannig, E.M., and Donahue, T.F. (1997). GTP hydrolysis controls stringent selection of the AUG start codon during translation initiation in Saccharomyces cerevisiae. Genes Dev *11*, 2396-2413.
Kabsch, W.J. (1988). Evaluation of single crystal X-ray diffraction data from a position sensitive detector. J Appl Crystallogr *21*, 916-924.
Laskowski, R.A., Mac Arthur, M.W., Moss, D.S., and Thornton, J.M. (1993). PROCHECK: a program to check the stereochemical quality of protein structure. J Appl Crystallogr *26*, 283-291.
Liu, S., Chang, J.S., Herberg, J.T., Horng, M.M., Tomich, P.K., Lin, A.H. and Marotti, K.R. (2006). Allosteric inhibition of Staphylococcus aureus D-alanine:D-alanine ligase revealed by crystallographic studies. Proc Natl Acad Sci U S A *103*, 15178-15183.
Lorsch, J., and Dever, T. (2010). Molecular view of 43S complex formation and start site selection in eukaryotic translation initiation. J Biol Chem *285*, 21203-21207.
Miller, G.J., Wilson, M.P., Majerus, P.W., and Hurley, J.H. (2005). Specificity determinants in inositol polyphosphate synthesis: crystal structure of inositol 1,3,4-trisphosphate 5/6-kinase. Mol Cell *18*, 201-212.
Naveau, M., Lazennec-Schurdevin, C., Panvert, M., Dubiez, E., Mechulam, Y., and Schmitt, E. (2013). Roles of yeast eIF2alpha and eIF2beta subunits in the binding of the initiator methionyl-tRNA. Nucleic Acids Res *41*, 1047-1057.
Ohno, K., Okuda, A., Ohtsu, M., and Kimura, G. (1984). Genetic analysis of control of proliferation in fibroblastic cells in culture. I. Isolation and characterization of mutants temperature-sensitive for proliferation or survival of untransformed diploid rat cell line 3Y1. Somatic cell and molecular genetics *10*, 17-28.
Okuda, A., and Kimura, G. (1996). An amino acid change in novel protein D123 is responsible for temperature-sensitive G1-phase arrest in a mutant of rat fibroblast line 3Y1. Experimental cell research *223*, 242-249.
Pedulla, N., Palermo, R., Hasenohrl, D., Blasi, U., Cammarano, P., and Londei, P. (2005). The archaeal eIF2 homologue: functional properties of an ancient translation initiation factor. Nucleic Acids Res *33*, 1804-1812. Print 2005.
Perzlmaier, A.F., Richter, F., and Seufert, W. (2013). Translation initiation requires cell division cycle 123 (Cdc123) to facilitate biogenesis of the eukaryotic initiation factor 2 (eIF2). J Biol Chem *288*, 21537-21546.
Roll-Mecak, A., Alone, P., Cao, C., Dever, T.E., and Burley, S.K. (2004). X-ray structure of translation initiation factor eIF2gamma : implications for tRNA and eIF2alpha binding. J Biol Chem *279*, 10634-10642.

Roper, D.I., Huyton, T., Vagin, A., and Dodson, G. (2000). The molecular basis of vancomycin resistance in clinically relevant Enterococci: crystal structure of D-alanyl-D-lactate ligase (VanA). Proc Natl Acad Sci U S A *97*, 8921-8925.

Schmitt, E., Blanquet, S., and Mechulam, Y. (2002). The large subunit of initiation factor aIF2 is a close structural homologue of elongation factors. EMBO J *21*, 1821-1832.

Schmitt, E., Naveau, M., and Mechulam, Y. (2010). Eukaryotic and archaeal translation initiation factor 2: a heterotrimeric tRNA carrier. FEBS Lett *584*, 405-412.

Schmitt, E., Panvert, M., Lazennec-Schurdevin, C., Coureux, P.D., Perez, J., Thompson, A., and Mechulam, Y. (2012). Structure of the ternary initiation complex aIF2-GDPNP-methionylated initiator tRNA. Nat Struct Mol Biol *19*, 450-454.

Schrodinger, LLC (2010). The PyMOL Molecular Graphics System, Version 1.3r1.

Sloane, V., Blanchard, C.Z., Guillot, F., and Waldrop, G.L. (2001). Site-directed mutagenesis of ATP binding residues of biotin carboxylase. Insight into the mechanism of catalysis. J Biol Chem *276*, 24991-24996.

Soler Artigas, M., Loth, D.W., Wain, L.V., Gharib, S.A., Obeidat, M., Tang, W., Zhai, G., Zhao, J.H., Smith, A.V., Huffman, J.E*., et al.* (2011). Genome-wide association and large-scale follow up identifies 16 new loci influencing lung function. Nat Genet *43*, 1082-1090.

Stolboushkina, E., Nikonov, S., Nikulin, A., Blasi, U., Manstein, D.J., Fedorov, R., Garber, M., and Nikonov, O. (2008). Crystal structure of the intact archaeal translation initiation factor 2 demonstrates very high conformational flexibility in the alpha- and beta-subunits. J Mol Biol *382*, 680-691.

Storoni, L.C., McCoy, A.J., and Read, R.J. (2004). Likelihood-enhanced fast rotation functions. Acta Crystallogr *D60*, 432-438.

Yatime, L., Mechulam, Y., Blanquet, S., and Schmitt, E. (2006). Structural switch of the gamma subunit in an archaeal aIF2 alpha gamma heterodimer. Structure *14*, 119-128.

Yatime, L., Mechulam, Y., Blanquet, S., and Schmitt, E. (2007). Structure of an archaeal heterotrimeric initiation factor 2 reveals a nucleotide state between the GTP and the GDP states. Proc Natl Acad Sci U S A 104, 18445-18450.

Yatime, L., Schmitt, E., Blanquet, S., and Mechulam, Y. (2004). Functional molecular mapping of archaeal translation initiation factor 2. J Biol Chem *279*, 15984-15993.

Zeggini, E., Scott, L.J., Saxena, R., Voight, B.F., Marchini, J.L., Hu, T., de Bakker, P.I., Abecasis, G.R., Almgren, P., Andersen, G*., et al.* (2008). Meta-analysis of genome-wide association data and large-scale replication identifies additional susceptibility loci for type 2 diabetes. Nat Genet *40*, 638-645.

Zhao, G., Jin, Z., Wang, Y., Allewell, N.M., Tuchman, M., and Shi, D. (2013). Structure and function of Escherichia coli RimK, an ATP-grasp fold, L-glutamyl ligase enzyme. Proteins *81*, 1847-1854.

**FIGURE LEGENDS**

**Figure 1: Structure of Sp-Cdc123**

A-Schematic representation of the topology of Sp-Cdc123Δc. The β-strands are represented as arrows and the helices as rods. Secondary structure elements were assigned with PROCHECK (Laskowski et al., 1993). Domain 1 is colored in blue (residues 1-170) and domain 2 is colored in yellow (residues 171-274).

B-Cartoon representation of Sp-Cdc123Δc. Same color code as in view A. ADP is shown as sticks. Secondary structure elements are labeled. All structural views are drawn with PyMol (Schrodinger, 2010).

See also Figure S1.

**Figure 2: Comparison of sp-Cdc123 with D-alanyl-D-lactate ligase from ATP-grasp superfamily**

A-Left: cartoon representation of Sp-Cdc123Δc. Domain 1 is colored in blue and domain 2 is colored in yellow except for regions specific to Cdc123 proteins which are colored in green. ATP is shown in sticks. Right: cartoon representation of (VanA) from *Enterococcus faecium* (PDB ID Code 1E4E, (Roper et al., 2000)). For the sake of clarity, the N-terminal domain is not represented. Parts of the central domain of 1E4E similar to Cdc123 are colored in blue, parts of the C-domain of 1E4E similar to Cdc123 are colored in yellow. Divergent regions as compared to Cdc123 are shown in green. The small and large loops overhanging ATP are shown in orange. ATP and a phosphorylated inhibitor bound to VanA are shown in sticks and spheres. The Magnesium ion is shown as a green sphere.

B-Left: Close-up view of the domain 1 of Sp-Cdc123 showing the three stranded β-sheet. Right: Close-up view of the central domain of 1E4E showing the four-stranded β-sheet and the two loops surrounding ATP. The color code is the same as in panel A. This view highlights the differences within the ATP-binding site between Cdc123 and the representative from the ATP-grasp family.

See also Figure S2.

C-Superimposition of the ATP-grasp core domain of Cdc123 (in blue and yellow, as in view A) onto the corresponding one in 1E4E (in grey). For the sake of clarity, divergent regions have been omitted.

**Figure 3: Binding of ADP to Sp-Cdc123Δc**

A-The residues involved in ADP binding and the corresponding electrostatic bonds are shown. Color code is the same as in Figure 2A. Water molecules are in red spheres.

B-Molecular surface representation of Sp-Cdc123Δc. Color code is the same as in Figure 2A. The view highlights the second cavity facing the ATP binding pocket.

See also Figure S3.

**Figure 4:Structure of Sp-Cdc123:Sc-eIF2γDIII complex**

A-Overall structure of Sp-Cdc123:Sc- eIF2γDIII complex. Sp-Cdc123 is colored as in Figure 1B. ATP is shown with sticks and $Mg^{2+}$ with a green sphere. Sc-γDIII is shown in orange.

B-Solution studies using SAXS. The experimental SAXS curve (blue) is compared with the theoretical diffusion curve deduced from the crystalline structure of Sp-Cdc123:Sc-γDIII complex (red).

C-Close-up view of Sp-Cdc123:Sc-γDIII showing the proximity of the ATP-binding pocket with the interface between the two proteins.

D-Detailed interactions between Sp-Cdc123 and Sc-γDIII. The residues involved in the stabilization of the interface between the two proteins and the corresponding electrostatic interactions are shown (see also Table 2). The right view is rotated by 180° as compared to the left view.

See also Figure S4.

**Figure 5: Binding of ATP-$Mg^{2+}$ to Sp-Cdc123:Sc-γDIII complex**

A-The residues involved in ATP binding and the corresponding electrostatic interactions are shown. Color code is the same as in Figure 3A. Water molecules are in red spheres and the magnesium ion in green sphere.

B- Right panel: Failure of Cdc123-DIN (DIN266-268AAA) and Cdc123 D252A to support cell viability. Diploid yeast cells heterozygote for a *CDC123* gene deletion and expressing either a wild type copy of *CDC123* (upper panel; W14145), DIN (DIN266-268AAA; middle panel; W13936) or D252A (lower panel; W13935) mutant versions of CDC123 were sporulated and subjected to tetrad dissection. Left panel: Failure of Cdc123-DIN (DIN266-268AAA) and Cdc123 D252A to support interaction of eIF2γ with eIF2α. In yeast strains that overexpress a flag-tagged version of eIF2γ /Gcd11 and eIF2α /Sui2 and that carry either the endogenous wild type copy of *CDC123* (W7743; lane 1) or are deleted for *CDC123* (*cdc123-Δ*; lanes 2-5; W7745 lane 2) and express a wild type copy (W13930; lane 3), the DIN mutant version of *CDC123* (W13931; lane 4) or D252A (W14238; lane 5). Cdc123, eIF2γ and eIF2α were detected by Western analysis of whole cell extracts (WCE). Flag-tagged eIF2γ was immunoprecipitated (IP) and precipitates were analyzed for the presence of eIF2α (Co-IP). Flag-eIF2γ was precipitated and detected with the monoclonal flag antibody M2. Cdc123 and eIF2α were detected by rabbit antisera.

See also Figure S5.

**Figure 6: Model for the binding of Cdc123 to eIF2αγ**

A-Molecular surface representation of Sc-Cdc123: Sc-eIF2γDIII complex. Color code is the same as that used in Figure 4.

B-Docking of aIF2γ onto Sp-Cdc123.

Sc-eIF2γDIII domain from the Sp-Cdc123:γDIII structure, was superimposed on the corresponding domain in aIF2γ structure (4RD4, Dubiez et al., 2015). Sp-Cdc123:γDIII is colored as in view A. Domain I of aIF2γ is colored in green, domain II of aIF2γ is colored in red. An arrow indicates the long L1 loop responsible for the binding of aIF2γ to aIF2α (Yatime et al., 2006).

C-Docking of aIF2αγ onto Sp-Cdc123.

Sc-eIF2γDIII domain from the Sp-Cdc123:γDIII structure, was superimposed on the corresponding domain in aIF2αγ structure (see text, 2AHO, (Yatime et al., 2006)). Color code is the same as in view

B for aIF2γ and Cdc123. aIF2α is colored as follows: Domain 1 in dark blue, domain 2 in light blue and domain 3 in cyan.

On the right of the structural views are schematics illustrating domain contacts within models of Cdc123:eIF2γ and Cdc123:eIF2αγ complexes.

See also Figure S6.

Figure 1

A

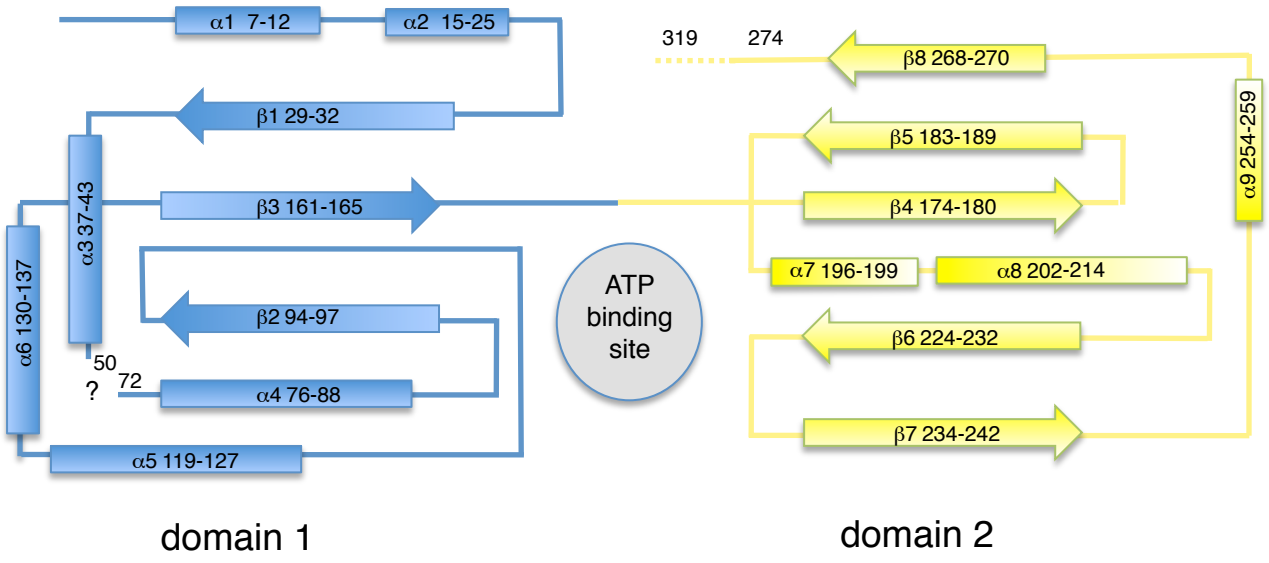
α1 7-12
α2 15-25
β1 29-32
α3 37-43
β3 161-165
α6 130-137
β2 94-97
50
?
72
α4 76-88
α5 119-127
ATP binding site
319
274
β8 268-270
β5 183-189
β4 174-180
α9 254-259
α7 196-199
α8 202-214
β6 224-232
β7 234-242
domain 1
domain 2

B

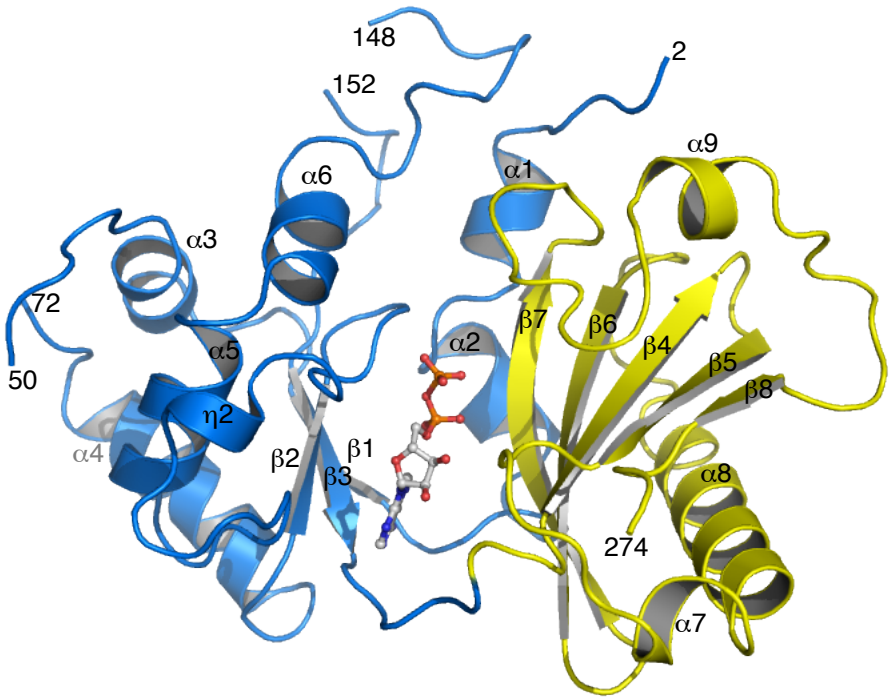
148
152
2
α9
α1
α6
α3
72
50
α5
α2
β7
β6
β4
β5
β8
η2
α4
β2
β1
β3
α8
274
α7

Figure 2

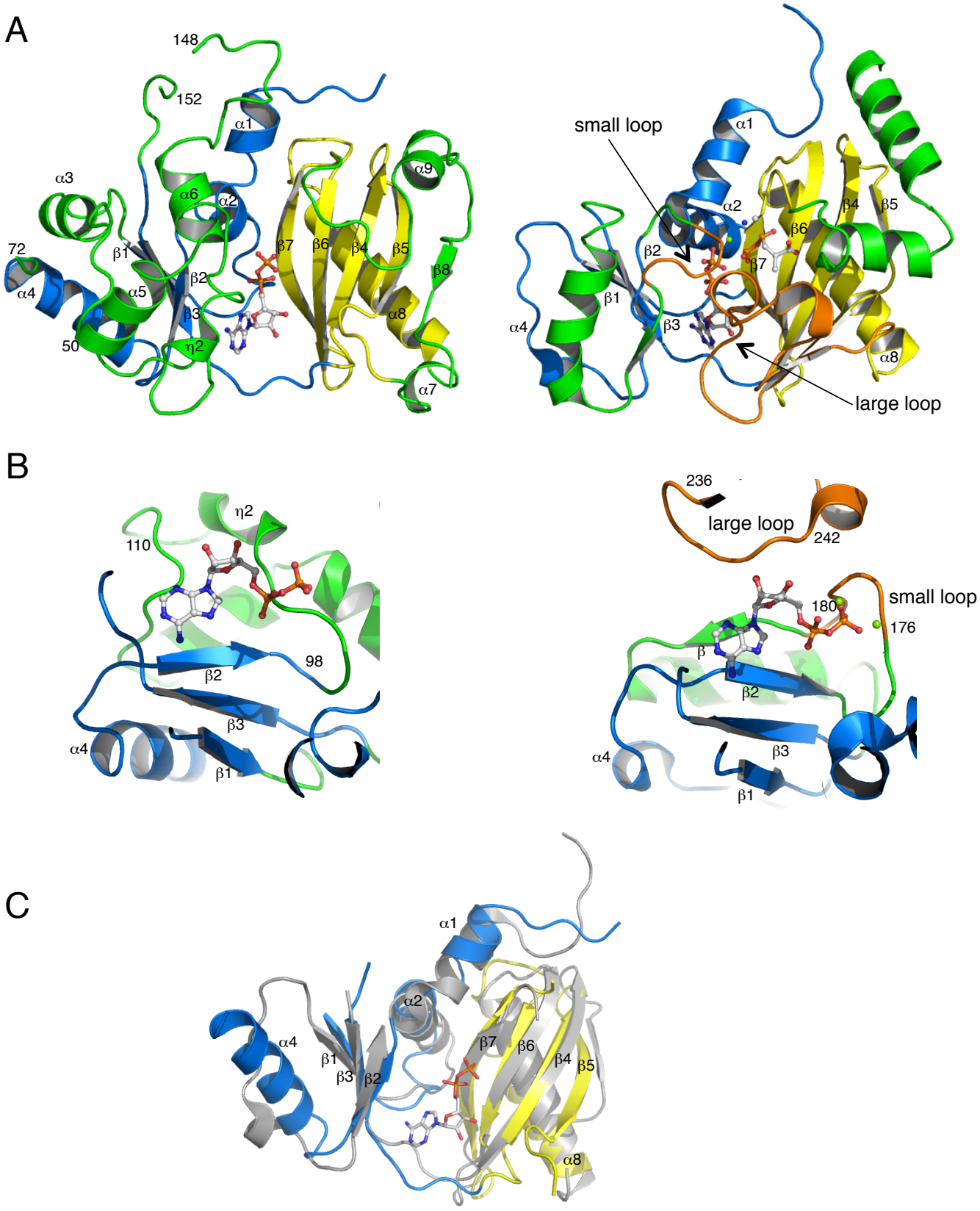
A
148
152
α1
α3
α6
α2
α9
72
β1
β7
β6
β4
β5
β8
α4
α5
β2
β3
α8
50
η2
α7
small loop
α1
α2
β4
β5
β6
β2
β7
β1
α4
β3
α8
large loop
B
η2
110
98
β2
β3
α4
β1
236
large loop
242
small loop
180
176
β
β2
α4
β3
β1
C
α1
α2
α4
β7
β6
β4
β5
β1
β3
β2
α8

Figure 3

A

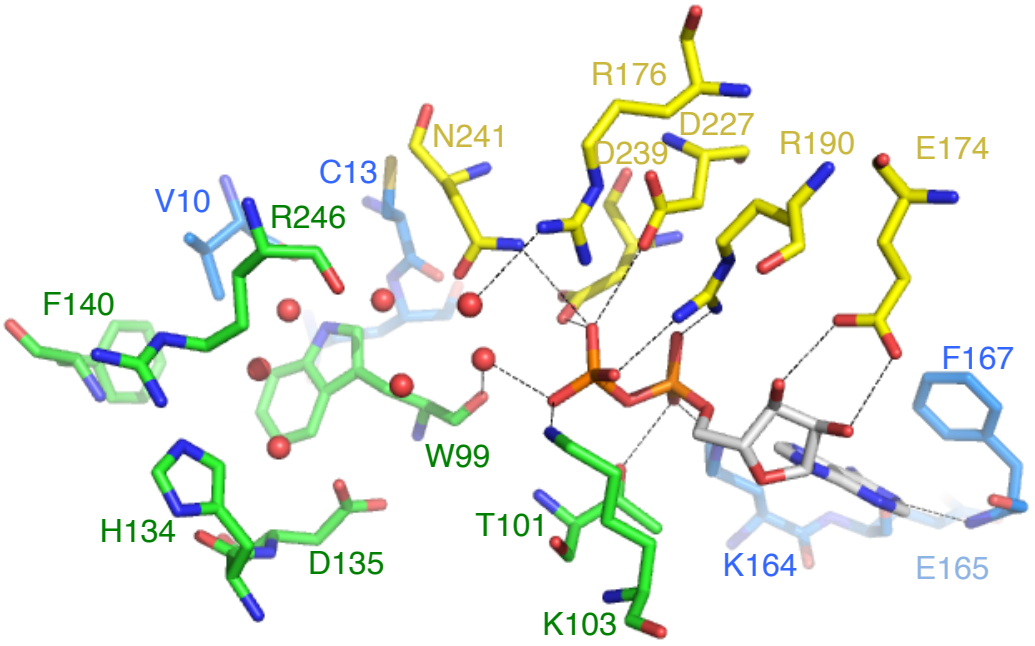
R176
N241
D227
D239
R190
E174
C13
V10
R246
F140
F167
W99
H134
D135
T101
K164
E165
K103

B

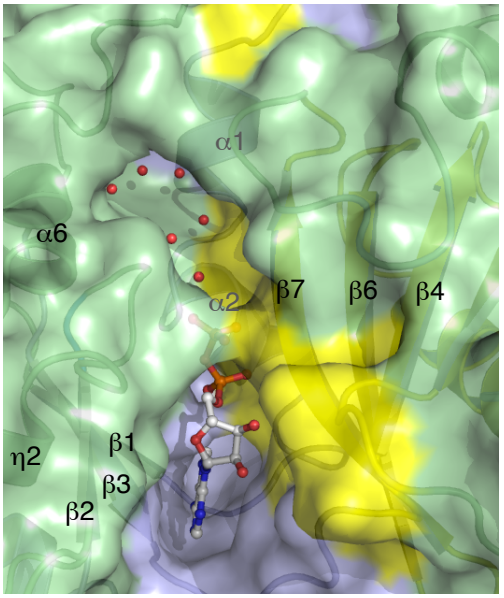
α1
α6
α2
β7
β6
β4
η2
β1
β3
β2

Figure 4

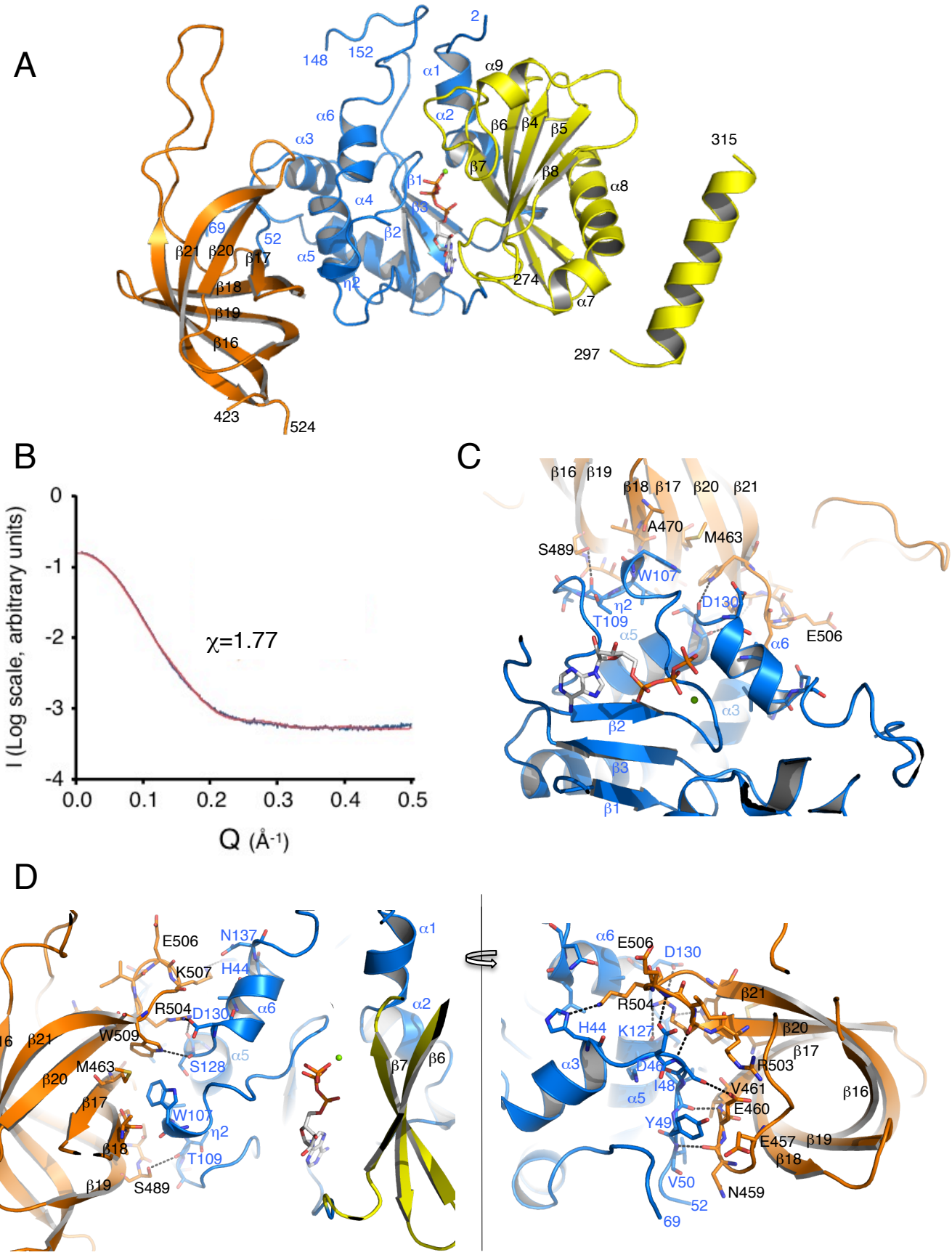
A
148
152
2
α1
α9
α6
α2
β6
β4
β5
α3
315
β7
β8
α8
β1
α4
β3
69
52
β2
β21
β20
β17
α5
274
β18
η2
α7
β19
297
β16
423
524
B
I (Log scale, arbitrary units)
0
-1
-2
-3
-4
χ=1.77
0.0
0.1
0.2
0.3
0.4
0.5
Q (Å-1)
C
β16
β19
β18
β17
β20
β21
A470
S489
M463
W107
D130
η2
T109
α5
α6
E506
α3
β2
β3
β1
D
E506
N137
K507
H44
α1
α2
R504
D130
α6
β16
β21
W509
α5
S128
β7
β6
M463
β20
β17
W107
η2
β18
T109
β19
S489
α6
E506
D130
β21
R504
H44
K127
β20
β17
α3
D46
R503
I48
V461
β16
α5
E460
Y49
E457
β19
β18
V50
N459
52
69

Figure 5

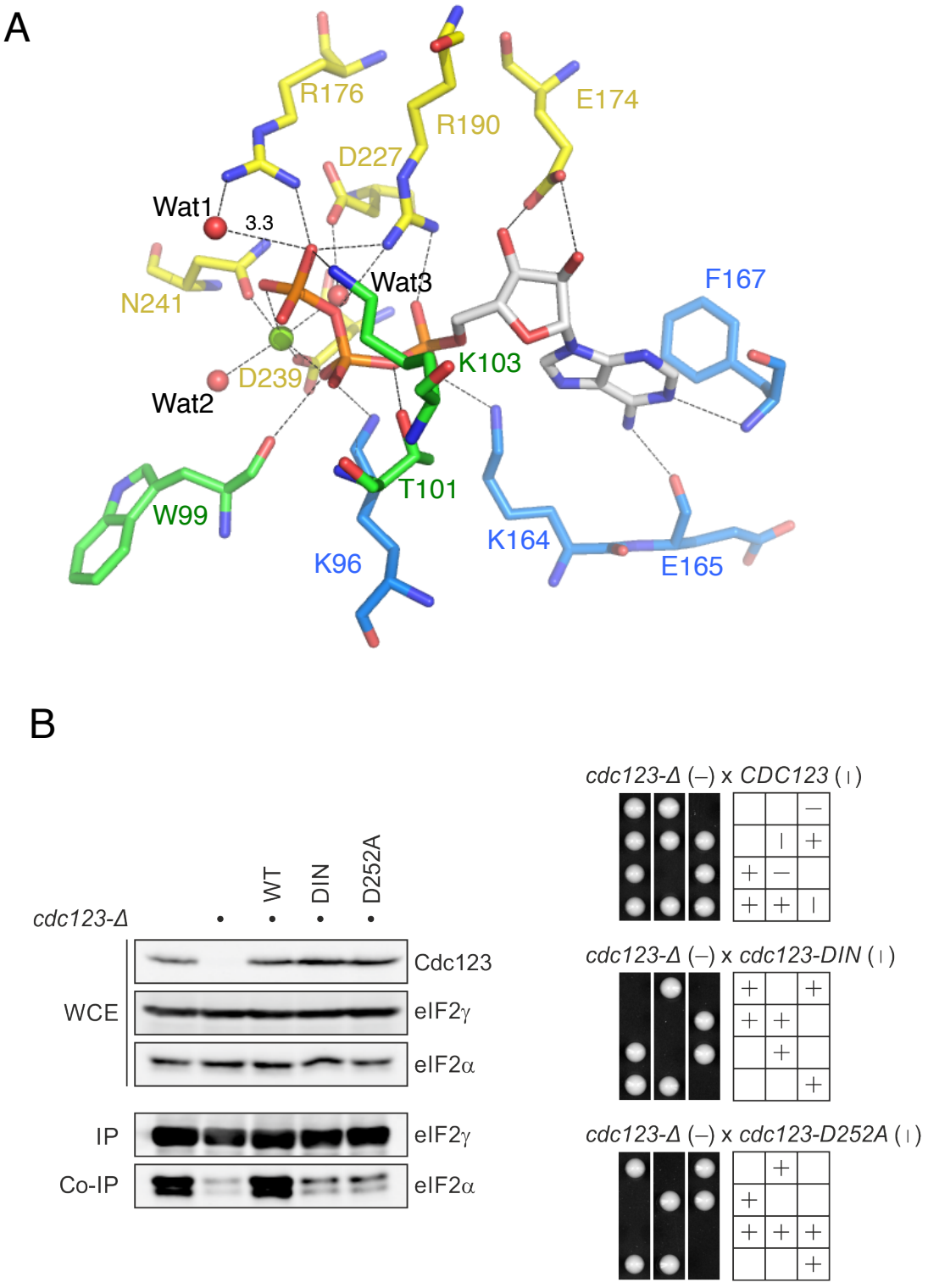
A
R176
R190
E174
D227
Wat1
3.3
Wat3
F167
N241
K103
D239
Wat2
T101
W99
K164
K96
E165
B
cdc123-Δ
WT
DIN
D252A
Cdc123
WCE
eIF2γ
eIF2α
IP
eIF2γ
Co-IP
eIF2α
cdc123-Δ (–) x CDC123 (+)
cdc123-Δ (–) x cdc123-DIN (+)
cdc123-Δ (–) x cdc123-D252A (+)

Figure 6

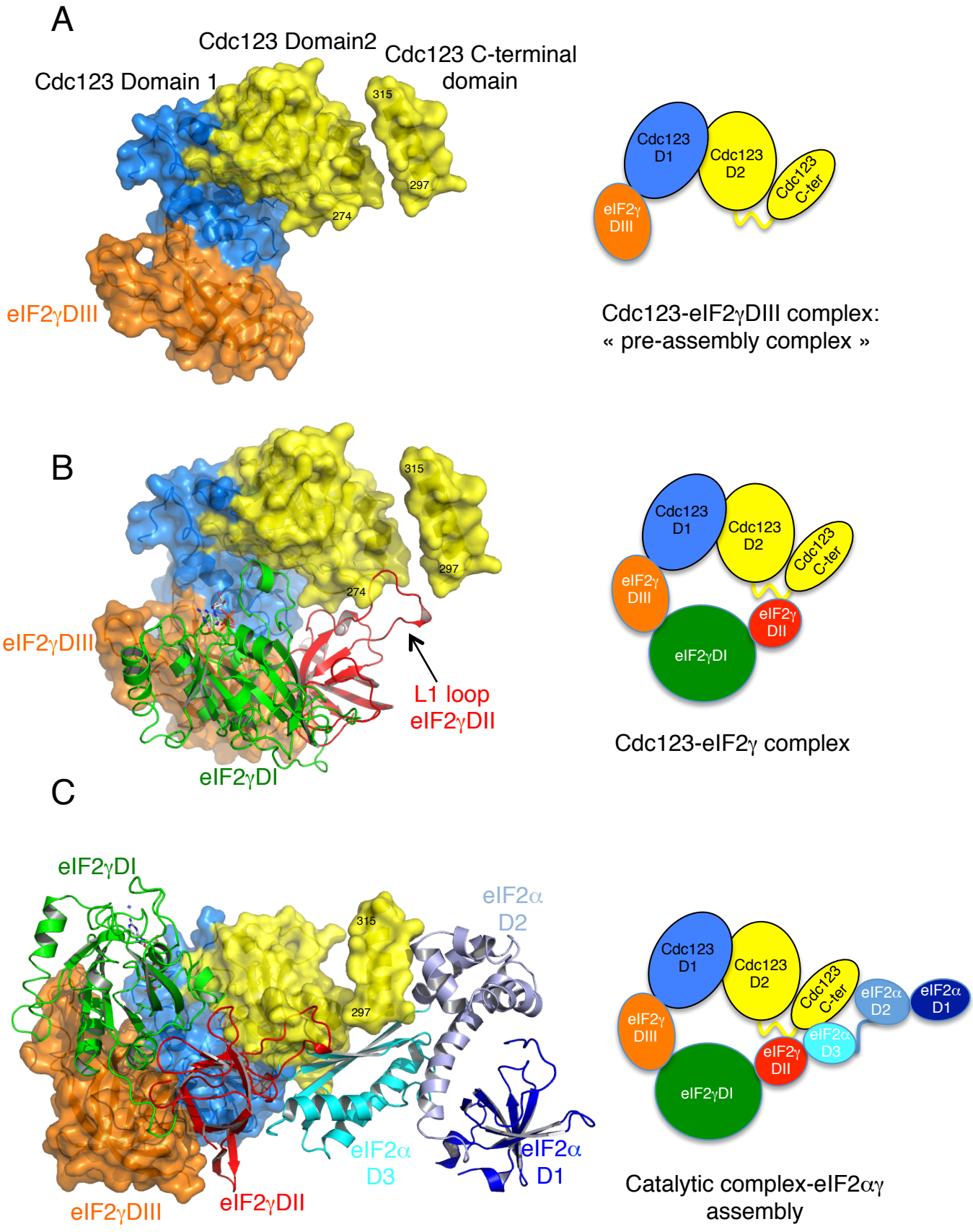
A
Cdc123 Domain2
Cdc123 C-terminal domain
Cdc123 Domain 1
315
297
274
eIF2γDIII
Cdc123 D1
Cdc123 D2
Cdc123 C-ter
eIF2γ DIII
Cdc123-eIF2γDIII complex:
« pre-assembly complex »
B
315
297
274
eIF2γDIII
L1 loop
eIF2γDII
eIF2γDI
Cdc123 D1
Cdc123 D2
Cdc123 C-ter
eIF2γ DIII
eIF2γ DII
eIF2γDI
Cdc123-eIF2γ complex
C
eIF2γDI
eIF2α D2
315
297
eIF2α D3
eIF2α D1
eIF2γDIII
eIF2γDII
Cdc123 D1
Cdc123 D2
Cdc123 C-ter
eIF2α D2
eIF2α D1
eIF2γ DIII
eIF2α D3
eIF2γ DII
eIF2γDI
Catalytic complex-eIF2αγ assembly

Table 1

| **Data Collection** | Sp-Cdc123Δc | Sp-Cdc123Δc +ADP | Sp-Cdc123:Sc-γDIII +ATP-$Mg^{2+}$ | Sp-Cdc123:Sc-γDIII |
|---|---|---|---|---|
| Crystallization Conditions | 4% tacsimate pH 5.0 12%PEG3350 | 4% tacsimate pH5.0 12%PEG3350 | 0.2M LiSO4 0.1M Tris pH 8.0 25%PEG3350 | 0.2M LiSO4 0.1M Tris pH 8.0 25%PEG3350 |
| Space group | C2 | C2 | $C222_1$ | $C222_1$ |
| Cell dimensions | | | | |
| *a*, *b*, *c* (Å) | 85.6 91.7 86.2 | 86.5 91.4 86.0 | 74.3 116.6 132.6 | 75.0 117.4 132.4 |
| $\alpha, \beta, \gamma$ (°) | 90 93.5 90 | 90 91.4 90 | 90 90 90 | 90 90 90 |
| Resolution (Å) | 45.8-2.06 | 43.2-1.85 | 45.0-2.9 | 45.7-3.0 |
| $R_{sym}$ (%) | 5.0 (90.8)[a] | 3.3 (47.4) | 7.4 (87.5) | 10.2 (117.3) |
| $I/\sigma I$ | 15.7 (1.3) | 19.0 (2.7) | 15.8 (2.2) | 13.4 (2.0) |
| CC1/2 (%) | 99.9 (77.5) | 99.9 (78.6) | 99.9 (80.4) | 99.9 (87.4) |
| Completeness (%) | 99.0 (94.3) | 98.1 (96.4) | 99.7 (99.3) | 99.6 (97.8) |
| Redundancy | 5.5 (5.1) | 3.0 (2.9) | 5.8 (5.9) | 7.3 (7.0) |
| | | | | |
| **Refinement** | | | | |
| Resolution (Å) | 45.8-2.06 | 43.2-1.85 | 45.0-2.9 | 45.7-3.0 |
| No. reflections | 41180 | 56270 | 13237 | 12020 |
| $R_{work}$ / $R_{free}$ | 0.193 (0.230) | 0.183 (0.221) | 0.195 (0.262) | 0.218 (0.257) |
| No. atoms/B-factors ($Å^2$) | | | | |
| Protein | Mono1Cdc123 2075/57.9 Mono2Cdc123 2060/66.4 | Mono1Cdc123 2096/35.5 Mono2Cdc123 2048/44.0 | Cdc123 2288/101.7 γD3 805/100.0 | Cdc123 2234/110.3 γD3 798/100.3 |
| Water | 198/62.5 | 331/44.3 | 5/72.8 | |
| Ligand | | ADP-mono1/27/38.4 | ATP 31/82.1 Mg 1/72.6 | |
| R.m.s. deviations | | | | |
| Bond lengths (Å) | 0.008 | 0.008 | 0.009 | 0.008 |
| Bond angles (°) | 1.09 | 1.10 | 1.18 | 1.05 |

**Table 1:** Data collection and refinement statistics for Sp-Cdc123 structure determination

A single crystal was used for data collection.

[a]Values in parentheses are for highest-resolution shell.

Table 2

| Sp-Cdc123 | Sc-γDIII | distances (Å) |
|---|---|---|
| | Electrostatic bonds | |
| H44 Nδ1 | K507 Nζ | 3.1 |
| D46 Oδ2 | E506 N (mc) | 3.0 |
| S47 Oγ | E460 Oε2 | 3.2 |
| I48 O (mc) | V461 N (mc) | 2.7 |
| V50 N (mc) | N459 O (mc) | 3.0 |
| S47 N (mc) | R504 O (mc) | 2.8 |
| K127 O | R504 Nh1 | 3.3 |
| D130 Oδ1 | R504 Nh2 | 2.7 |
| S128 O (mc) | W509 Nε | 3.3 |
| | Non-bonded contacts | |
| Y49 | E457 | |
| W107 | M463-A470-T471- G472 | |
| I108 | T488-S489 | |
| T109 | T488-S489 | |
| T110 | T488-S489 | |
| A133 | K507 | |
| L136 | K507 | |
| N137 | K507 | |
| L43 | K507 | |
| S47 | R503 | |
| D46 | I505 | |

**Table 2:** Summary of interactions involved in the binding of γDIII domain to Cdc123. Residue names are colored according to Figure S2.

Table 3

| Sp-Cdc 123 | ATP binding Sp-Cdc123:Sc-γDIII | distances (Å) |
|---|---|---|
| | Electrostatic bonds | |
| K96 Nζ | O1α | 2.9 |
| | O2β | 3.3 |
| T101 Oγ1 | O3α | 3.0 |
| | O1β | 2.8 |
| K164 Nζ | O1α | 2.8 |
| | N7 adenine | 2.9 |
| E165 O (mc) | N6 adenine | 3.0 |
| F167 N (mc) | N1 adenine | 3.2 |
| E174 Oε1 | O2' ribose | 3.3 |
| Oε2 | O3' ribose | 2.9 |
| R176 | O3γ | 3.0 |
| R190 Nh1 | O2α | 2.8 |
| Nh2 | O3γ | 2.9 |
| D227 Oδ2 | Wat3 | 2.7 |
| D239 Oδ2 | $Mg^{2+}$ | 2.1 |
| | O2β | 2.9 |
| N241 Oδ1 | $Mg^{2+}$ | 2.2 |
| Wat2 | $Mg^{2+}$ | 2.7 |
| Wat3 | $Mg^{2+}$ | 2.5 |
| | Non-bonded contacts | |
| K103 | O1γ | |
| | O1β | |
| S100 | O1γ | |
| | O1β | |
| I238 | O1β | |
| | O2β | |
| L114 | O4' ribose | |
| W166 | N6 adenine | |
| | N1 adenine | |
| | C2 adenine | |
| V94 | N6 adenine | |
| M169 | C8 adenine | |
| | N7 adenine | |
| | C5 adenine | |

**Table 3:** Summary of interactions involved in the binding of ATP to Sp-Cdc123:Sc-γDIII.

Residue names are colored according to Figure S2.

# Supplemental Data

## Supplemental Figures and Legends

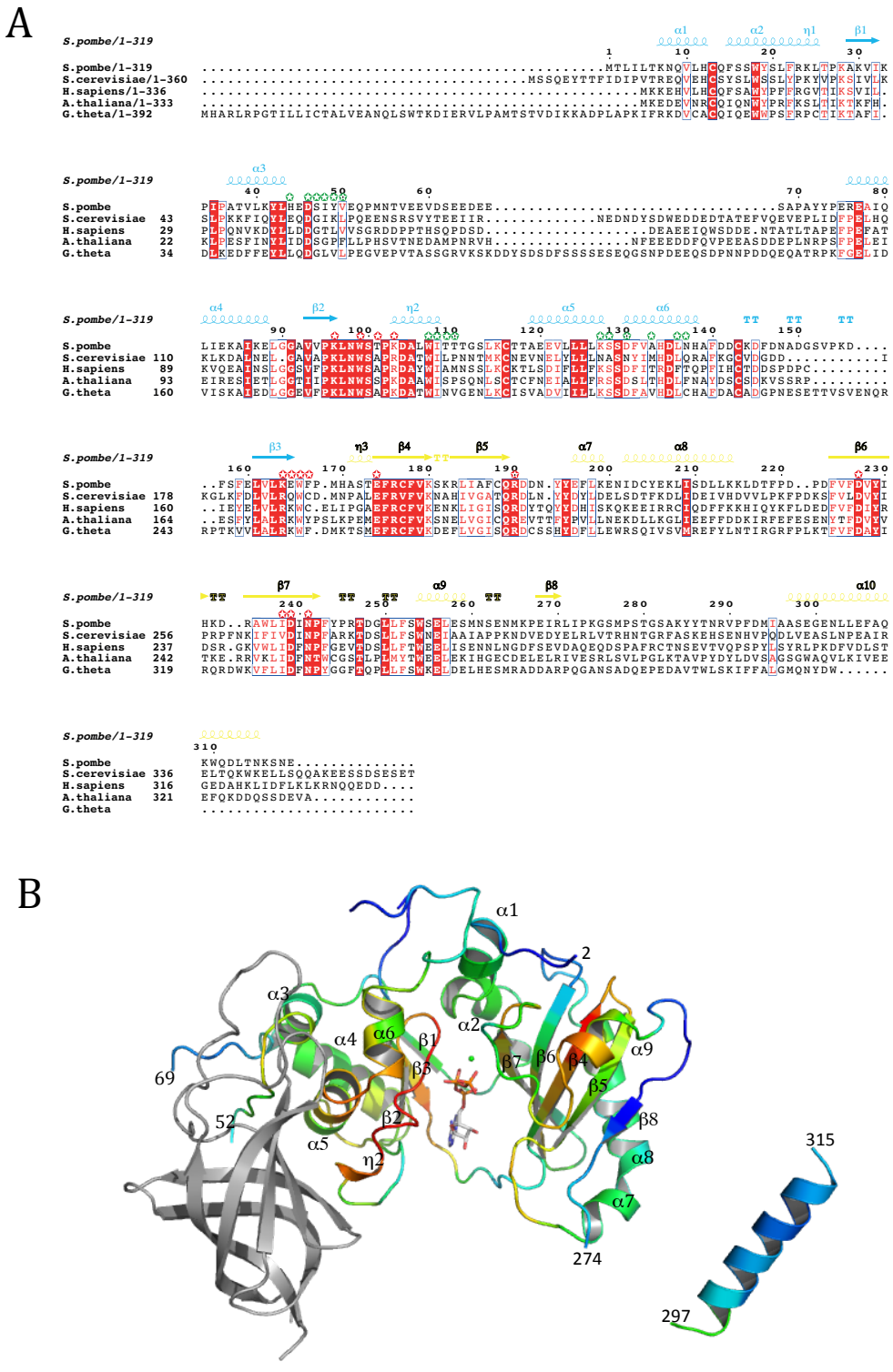


**Figure S1: Sequence conservation among Cdc123 orthologs**

A-*c.a* 200 sequences of Cdc123 orthologs were aligned using ClustalW (Larkin et al., 2007). The consensus sequence was calculated using JalView (Waterhouse et al., 2009). The figure was drawn

with Espript (Gouet et al., 1999) and edited manually. For the sake of clarity, only five representative Cdc123 sequences are shown. Residues conserved in 78-100% of the sequences are in white letters in red boxes. Residues conserved in 50-77% of the sequences are in red letters and boxed. Residues involved in ATP binding to Sp-Cdc123 are indicated with stars boxed in red. Residues involved in the binding of Sc-γDIII domain to Sp-Cdc123 are indicated with stars boxed in green. Secondary structures of Sp-Cdc123 are shown at the top of the alignment.

B-From the above alignment, conservations at each position were analyzed by using Jalview. The PAM 250 similarity matrix was used in this step. Residues on Cdc123 were colored according to the similarity score with a linear scale from blue to red (rainbow scale of PyMol). The γDIII domain was colored in grey.

A

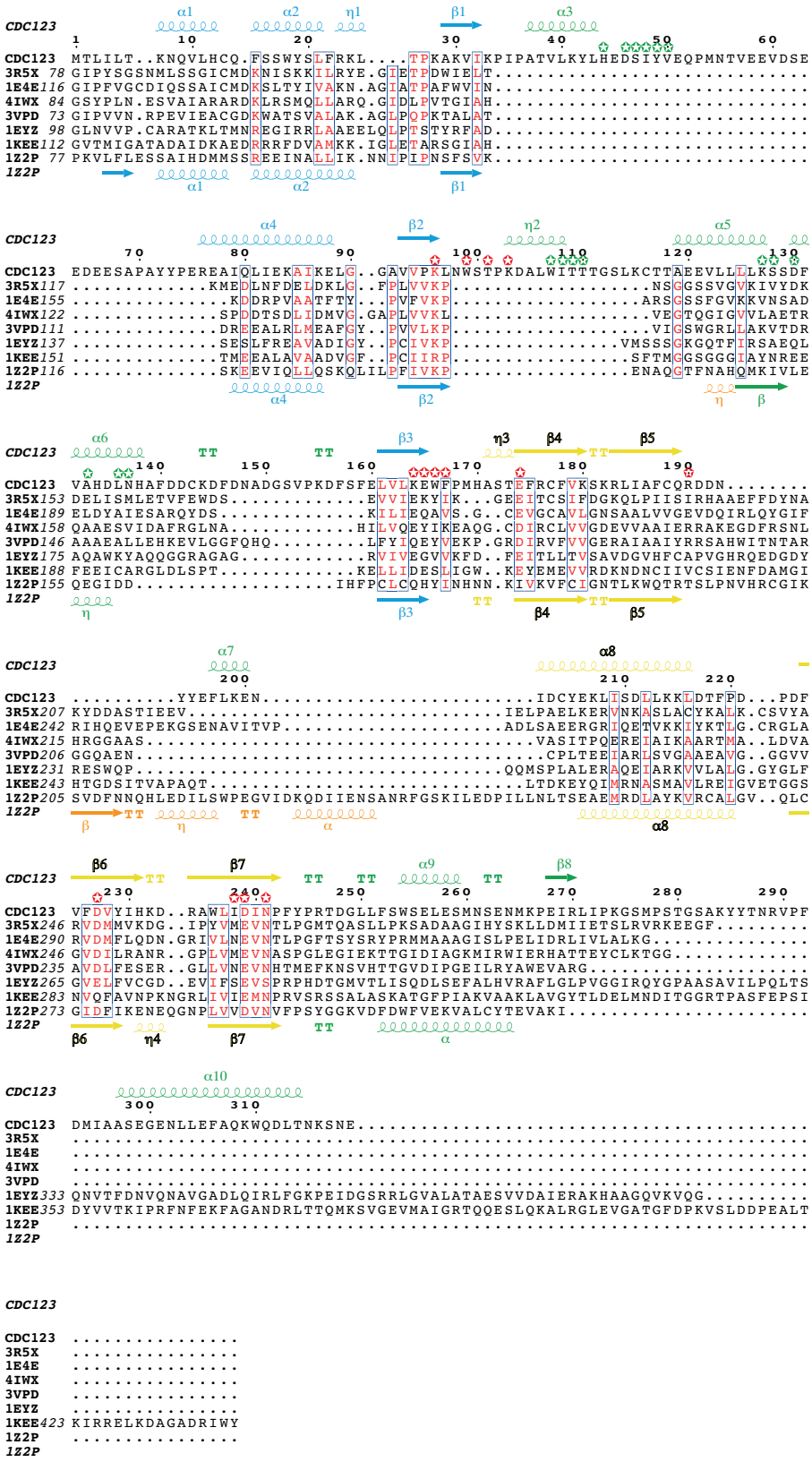

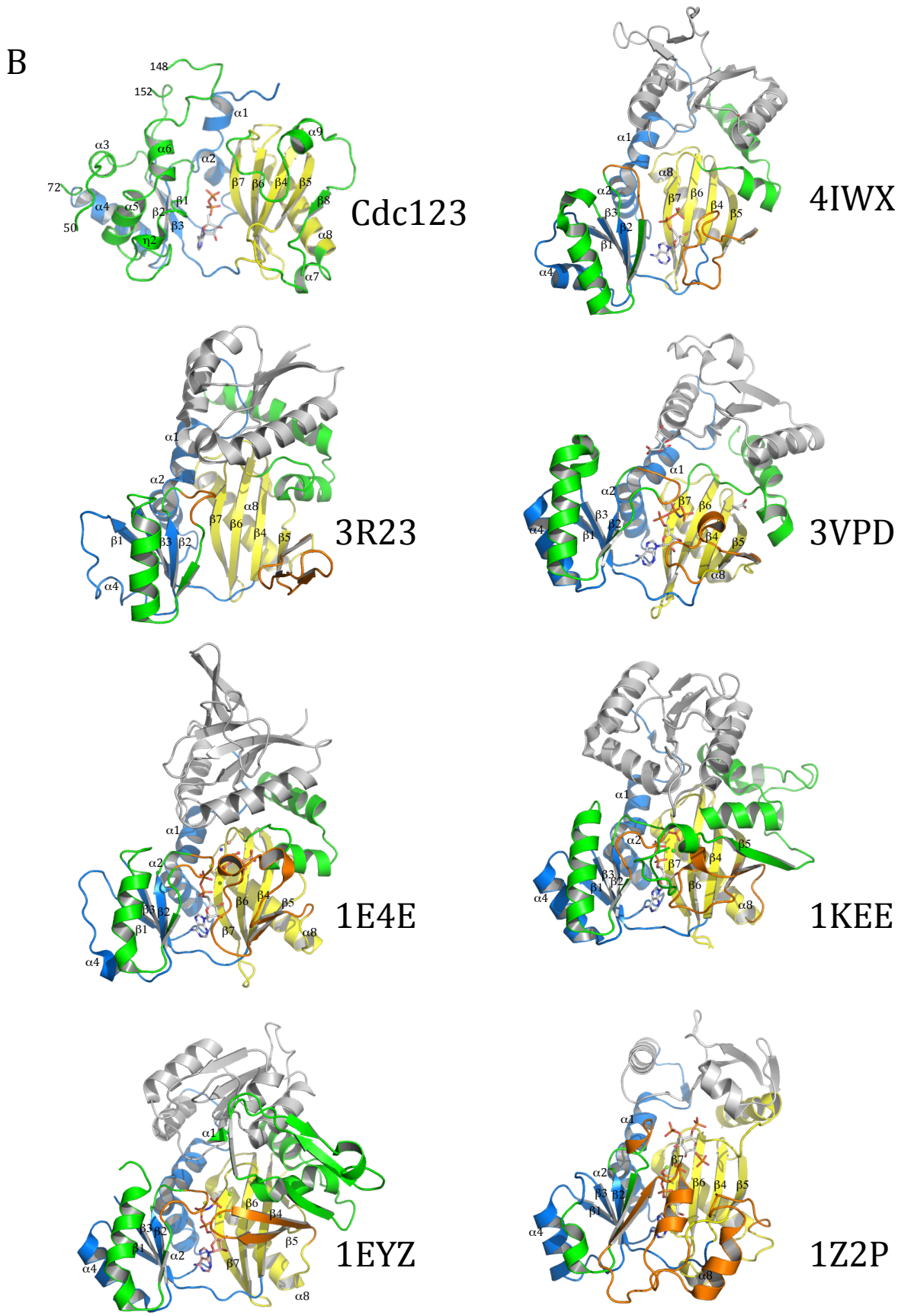


**Figure S2: Structural alignment of sp-Cdc123 with enzymes from ATP-grasp superfamily**

A- The sequence of Sp-Cdc123 was aligned to those of some ATP-Grasp enzymes according to the structural superimpositions. Secondary structure of Sp-Cdc123 is indicated at the top of the alignment. Secondary structure of Inositol 1,3,4-trisphosphate 5/6-Kinase (PDB ID code1Z2P; (Miller et al., 2005)) is indicated at the bottom of the alignment. Color code for the secondary structure elements is the same as in Figures 2 and S4. Conserved residues are boxed and colored in red. Residues involved in ATP binding to Sp-Cdc123 are indicated with stars boxed in red. Residues involved in the binding of Sc-γDIII domain to Sp-Cdc123 are indicated with stars boxed in green. The figure was drawn with Espript (Gouet et al., 1999). Sequences are labeled according to the ID code of the corresponding PDB entry.

B- Structural comparison of sp-Cdc123 with enzymes belonging to the ATP-grasp superfamily. Color code is as follows: in Cdc123, domain 1 is colored in blue and domain 2 is colored in yellow. In ATP-Grasp enzymes, domain N is colored in grey, the central domain is colored in blue and the C-terminal domain is colored in yellow. Divergent regions in Cdc123 and ATP-grasp are shown in green. Ligands are shown with sticks when available. The small and large loops overhanging ATP in ATP-Grasp are shown in orange. Regions specific to Cdc123 proteins are colored in green. ATP is shown in sticks. Secondary structures common to Cdc123 and ATP-grasp are labeled. The PDB code of each represented ATP-grasp structure is indicated on the right of the cartoon. 4IWX, RimK , (Zhao et al., 2013) $rms_d$ of 3.6 Å over 156 Cα atoms (Z=8.3); 3R23, D-alanine-D-alanine ligase, $rms_d$ of 3.2 Å over 160 Cα atoms (Z=11.2); 3VPD, LysX, (Ouchi et al., 2013) $rms_d$ of 3.7 Å over 160 Cα atoms (Z=9.6); 1E4E, D-alanyl-D-lactate ligase (Roper et al., 2000) $rms_d$ of 3.6 Å over 169 Cα atoms (Z=9.7); 1KEE, carbamoyl phosphate synthetase (Miles et al., 2002) $rms_d$ of 3.3 Å over 179 Cα atoms (Z=9.1); 1EYZ, Glycimanide ribonucleotide transformylase (Thoden et al., 2000) $rms_d$ of 3.3 Å over 175 Cα atoms (Z=9.1); 1Z2P, Inositol 1,3,4-trisphosphate 5/6-Kinase (Miller et al., 2005) $rms_d$ 3.1 Å over 166 Cα atoms (Z=10.0).

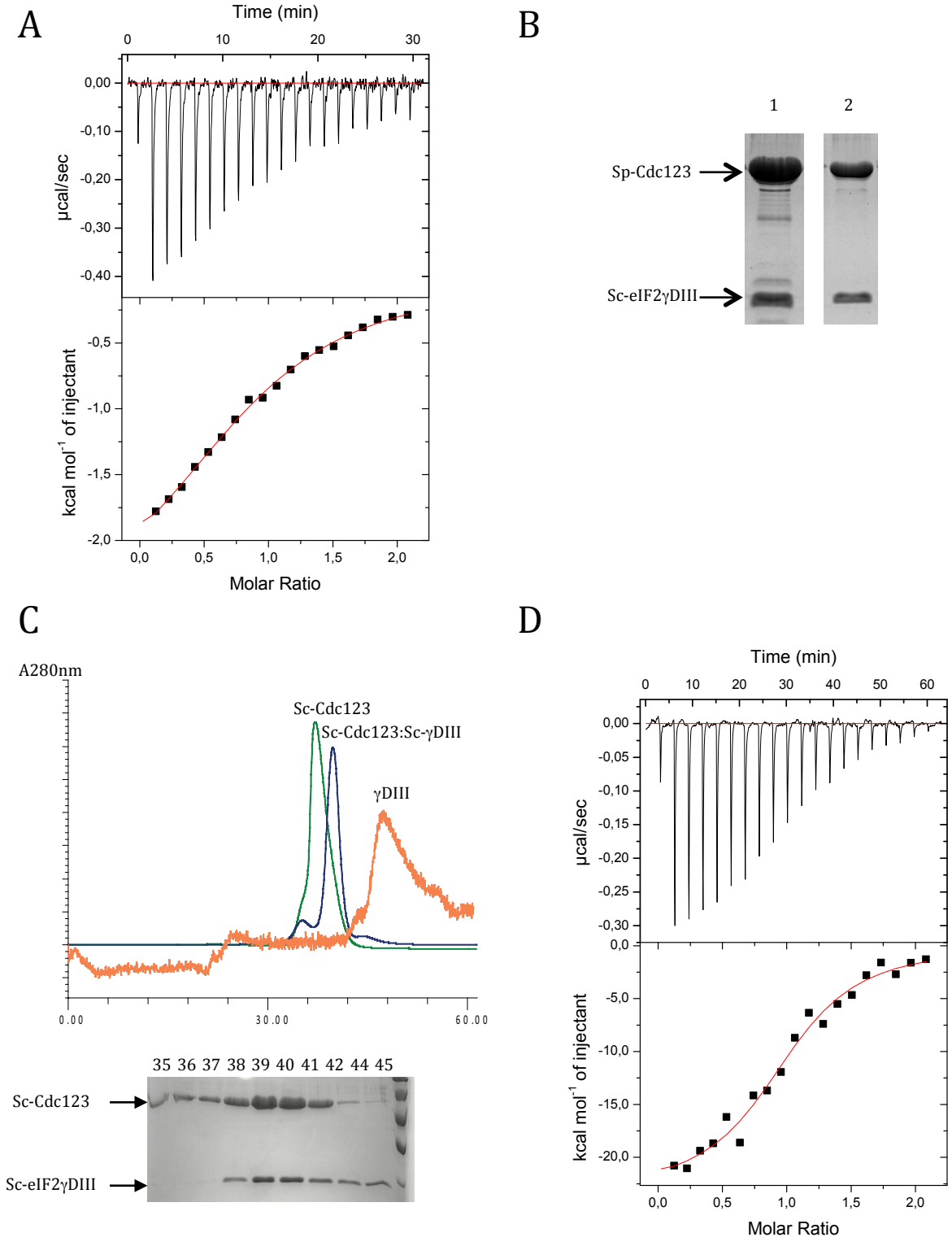


**Figure S3: Biochemical characterization of Cdc123**

A-Titration curve (upper panel) and binding isotherm (lower panel) of Sp-Cdc123 interaction with ATP-$Mg^{2+}$ at 25°C. The Kd value derived from the curve is 67 ± 13 µM.

B-SDS-PAGE analysis of the purification of the Sp-Cdc123:Sc-γDIII complex. Lane 1: sample obtained after the affinity chromatography step. Lane 2: sample obtained after molecular sieving.

C-Upper part: Overlay of elution profiles on molecular sieve (Superdex 200 HR 10/30) of Sc-Cdc123 (green), Sc-Cdc123:Sc-γDIII complex (blue) and Sc-γDIII (orange). Lower part: SDS-PAGE analysis of elution profile of Sc-Cdc123:Sc-γDIII complex (blue curve in upper panel). The number of each fraction is indicated (one fraction was collected every minute, 0.4 mL/min flow rate).

D-Titration curve (upper panel) and binding isotherm (lower panel) of Sc-Cdc123 interaction with Sc-γDIII at 25°C. The Kd value derived from the curve is 2.5 ± 0.5 µM.

A

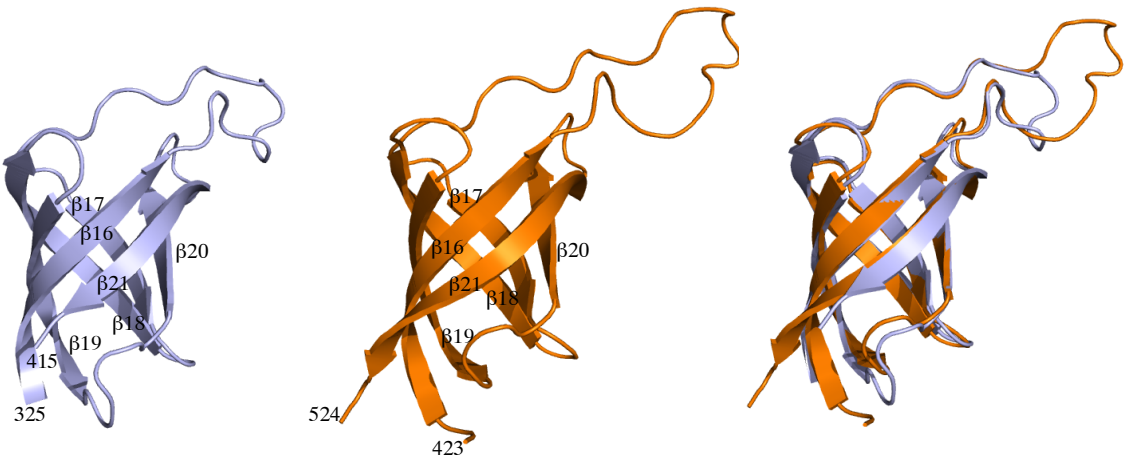


B

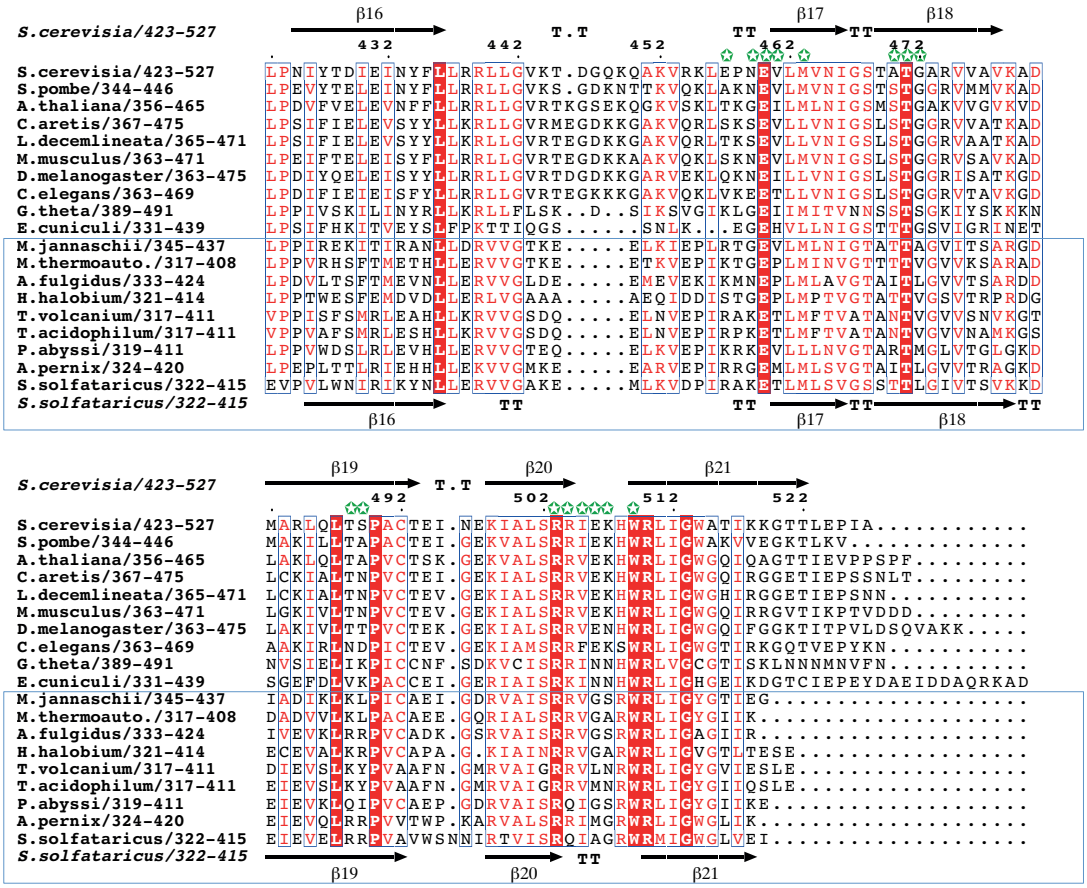


C

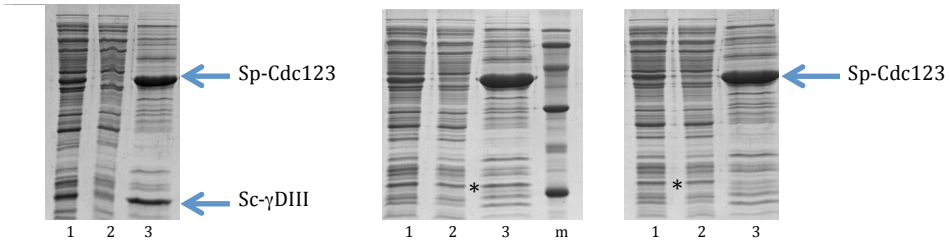


wt-Sc-γDIII R504A-Sc-γDIII W509A-Sc-γDIII

**Figure S4: e/aIF2γDIII domain.**

A-Cartoon representation of the γDIII domain. Left part: aIF2γDIII domain from *S. solfataricus* (PDB ID Code 2AHO, (Yatime et al., 2006)) colored in light blue. Middle part: eIF2γDIII domain from S. cerevisae as determined in this study, colored in orange. Right part: Superimposition of both structures ($rms_d$=0.69Å over 79 Cα atoms). Secondary structures are labeled according to (Yatime et al., 2006).

B-Alignment of e/aIF2-**γ**DIII domains sequences. 10 sequences of eukaryotic eIF2γ and 9 sequences of archaeal aIF2γ (framed in blue) were aligned using ClustalW (Larkin et al., 2007). The figure was drawn with Espript (Gouet et al., 1999). When the percentage of identity is higher that 70%, residues are colored in red and framed in blue. In case of strict identity, residues are in white on a red background. Residues involved in the binding of Sc-γDIII domain to Sp-Cdc123 are indicated with stars boxed in green. Secondary structures of Sc-γDIII are indicated at the top of the alignment and those of Ss-aIF2-γDIII are indicated at the bottom.

C- Binding assay of Sc-γDIII to Sp-Cdc123.

The pull-down binding assay is described in the Material and Methods section. An equal aliquot of each step of the batch purification (Talon affinity resin) was loaded onto a 12% polyacrylamide SDS gel. Stars indicate the position of Sc-γDIII.

Lane 1: soluble fraction of the crude extract

Lane 2: flow-through fraction of the batch purification

Lane 3: elution fraction of the batch purification

M:molecular weight marker (97, 67, 43, 30, 20, 14 kDa; GE Healthcare)

The views show that R504 and W509 mutants have lost some ability to bind Sp-Cdc123.

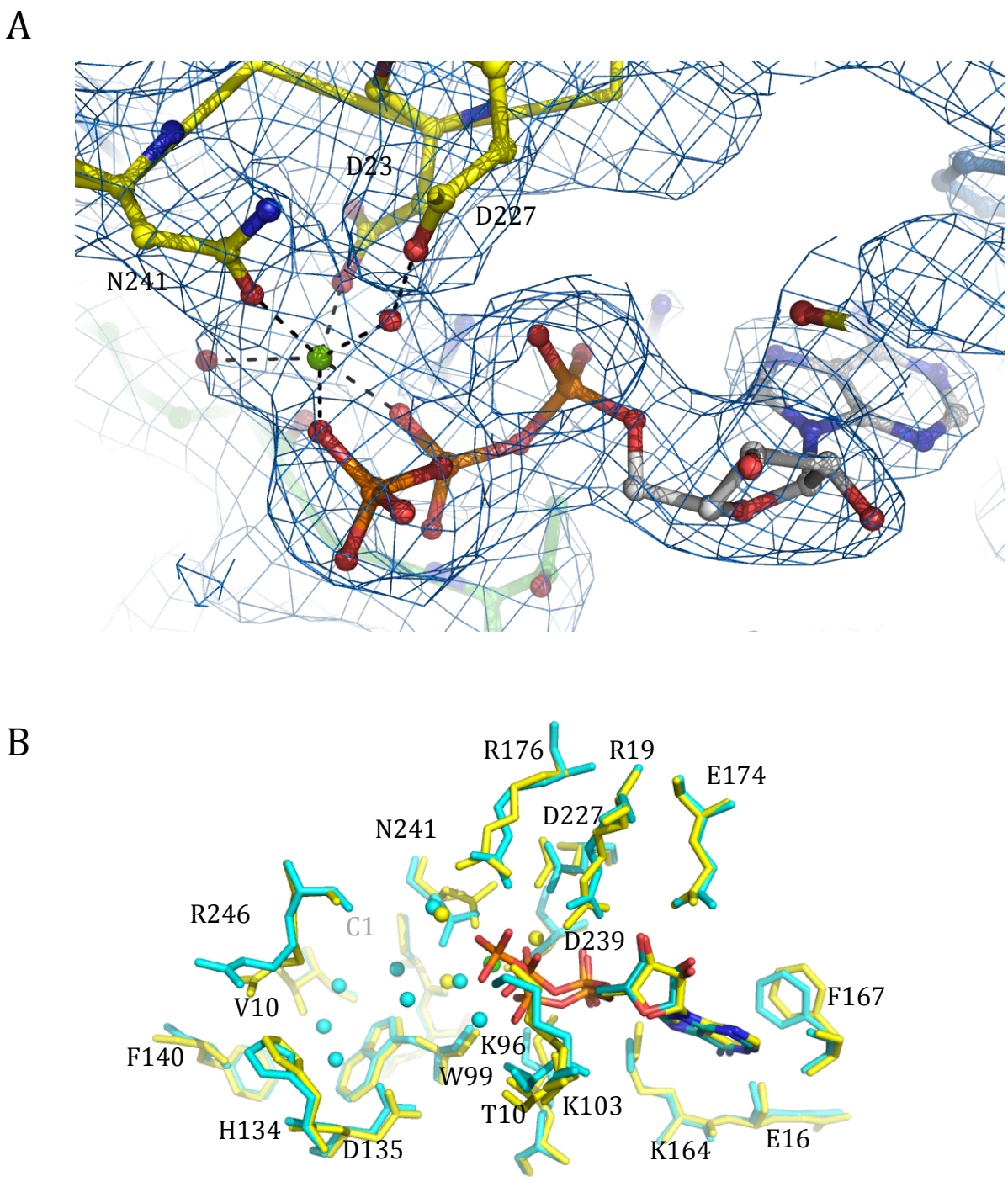


**Figure S5: Binding of ATP in Sp-cdc123:Sc-eIF2γDIII complex**

A- View of the 2.9 Å '2mFo-DFc' map of the Sp-cdc123:Sc-eIF2γDIII complex contoured at 1.0 standard deviation. Magnesium ion and water molecules are shown as green and red spheres, respectively. The view shows the coordination sphere of the magnesium ion involving the three highly conserved residues D227, D239 and N241 (Figure S1). B- Superimposition of the Sp-Cdc1223ΔC:ADP structure on that of Sp-cdc123:Sc-eIF2γDIII:ATP-$Mg^{2+}$ structure. Residues of Sp-

cdc123:Sc-eIF2γDIII:ATP-$Mg^{2+}$ are colored in yellow and those of Sp-Cdc1223ΔC:ADP are in cyan. Magnesium ion is shown as a green sphere and water molecules as yellow and cyan spheres.

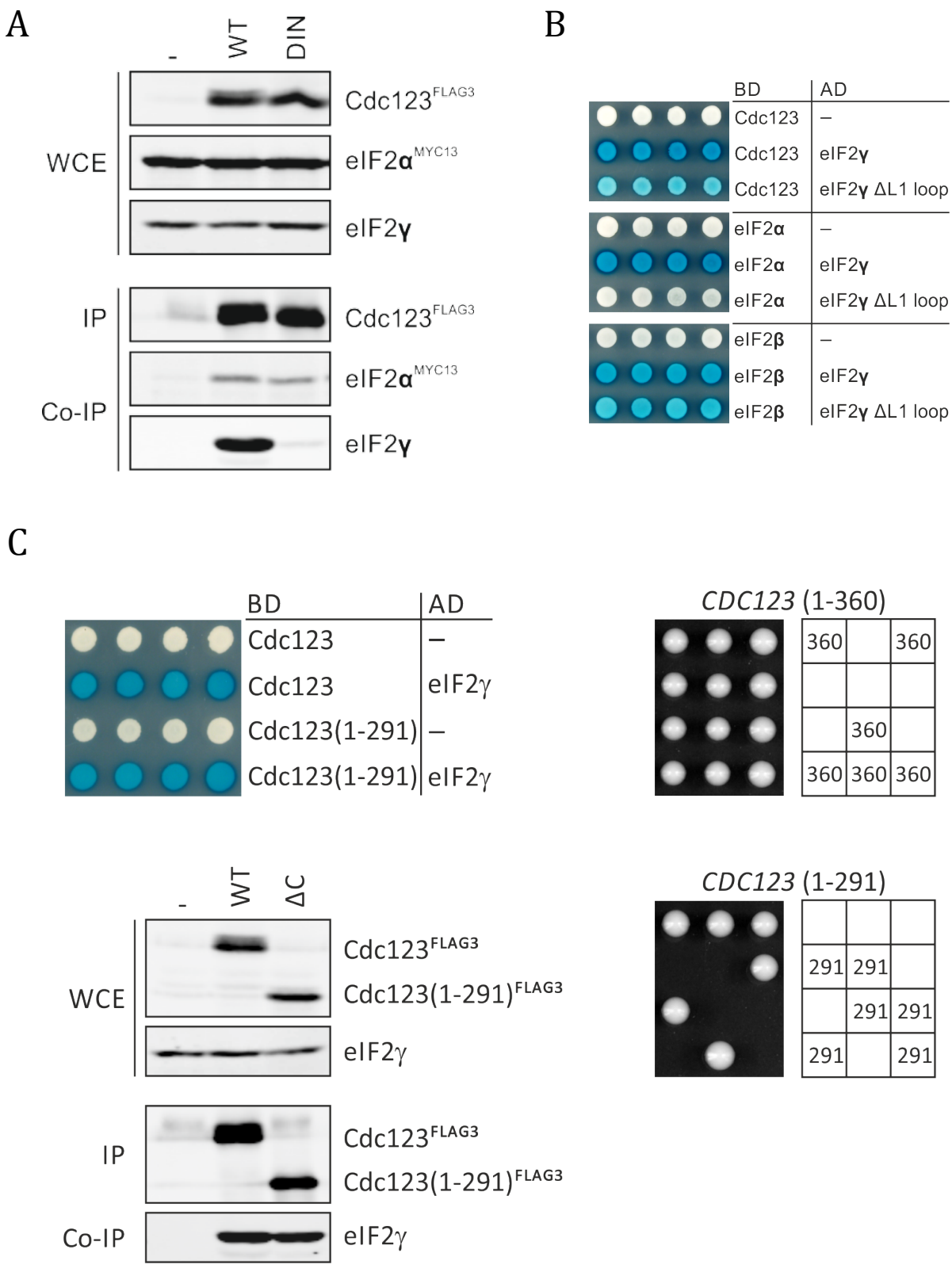


**Figure S6: Interaction of Sc-Cdc123 with eIF2 subunits and role of the C-terminal domain**

A- Interaction of Cdc123 with eIF2α and γ subunits.

Immunoprecipitates of Cdc123 and Cdc123-DIN were analyzed for co-precipitation of eIF2α and eIF2γ in yeast strains that express a myc-tagged version of eIF2α and overexpresses from the *TEF2* promoter a flag-tagged version of Cdc123 (WT) (W14185) or Cdc123-DIN (DIN) (W14186). A strain that expresses a myc-tagged version of eIF2α but lacks a flag-tagged version of Cdc123 (-) (W9876) was included as a negative control. Protein levels were determined by Western analysis in yeast whole cell extracts (WCE). Immunoprecipitates (IP) of Cdc123-flag and Cdc123-DIN-flag were prepared and analyzed for the presence of eIF2α and eIF2γ (Co-IP). For precipitation and detection of Cdc123-flag and Cdc123-DIN-flag the mouse monoclonal antibody M2 was used. eIF2α-myc and eIF2γ were detected by the mouse monoclonal antibody 9E10 and a rabbit antiserum to eIF2γ (Perzlmaier et al., 2013), respectively. Relative to eIF2γ, much lower amounts of eIF2α co-precipitated with Cdc123. The DIN mutation of Cdc123 reduced the interaction of Cdc123 with eIF2γ, but had little or no effect on the interaction of Cdc123 with eIF2α.

B- Role of the L1 loop of eIF2γ in the interaction of eIF2γ with Cdc123, eIF2α and eIF2β.

A yeast-two-hybrid assay was used to evaluate the consequences of deleting part of the L1 loop of eIF2γ (Sc-eIF2γ/Gcd11 aa325-331) on the ability of eIF2γ to associate with Cdc123 and eIF2 subunits. The reporter strain W276 was co-transformed with the indicated combination of a pEG202-derived DNA binding domain (BD) plasmid (BD-Cdc123: pWS1463; BD-eIF2α: pWS1537; BD-eIF2β: pWS1535) and a pJG4-5-derived transcriptional activation domain (AD) plasmid (AD -: pJG4-5; AD-eF2γ: pWS1513; AD-eIF2γ ΔL1 loop: pED002). The yeast-two-hybrid vector plasmids pEG202 and pJG4-5 have been described (Ausubel et al., 2005). Yeast colonies were overlayed with an X-gal top agar to visualize β-galactosidase reporter activation. The L1 loop deletion of eIF2γ reduced the interaction of eIF2γ with Cdc123 and prevented any interaction with eIF2α, but had little or no effect on the interaction with eIF2β.

C- Role of the C-terminal domain of Cdc123

A C-terminal truncation mutant of Cdc123 (Cdc123(1-291) lacking 69 amino acids from the C-terminus) was analyzed for its ability to interact with eIF2γ and support cell viability.

Left upper panel- Yeast-two-hybrid analysis of the Cdc123-eIF2γ interaction. The reporter strain W276 was co-transformed with the indicated combination of a pEG202-derived DNA binding domain (BD) plasmid (BD-Cdc123: pWS1463; BD-Cdc123(1-291): pWS3801) and a pJG4-5-derived transcriptional activation domain (AD) plasmid (AD -: pJG4-5; AD-eF2γ: pWS1513). The yeast-two-hybrid vector plasmids pEG202 and pJG4-5 have been described (Ausubel et al., 2005). Yeast colonies were overlayed with an X-gal top agar to visualize β-galactosidase reporter activation.

Left lower panel- Co-immunoprecipitation analysis of the Cdc123-eIF2γ interaction. Strains expressing flag-tagged versions of Cdc123 (WT; W14236) or Cdc123(1-291) (ΔC; W14237) from the regulable *GAL1* promoter were used for preparation of whole cell extracts (WCE), anti-flag immunoprecipitation (IP) and analysis of co-precipitation (Co-IP) of eIF2γ. A strain lacking a flag-tagged version of Cdc123 (-; W9878) was used as a negative control. Cdc123-flag, Cdc123(1-291)-flag and eIF2γ protein levels were detected by Western analysis of whole cell extracts (WCE). Cdc123-flag and Cdc123(1-291)-flag were immunoprecipitated (IP) and detected with the mouse monoclonal flag antibody M2. The precipitates were analyzed for co-precipitation of eIF2γ (Co-IP) using a rabbit antiserum to eIF2γ (Perzlmaier et al., 2013).

Right panels- Tetrade dissection analysis for evaluating the biological function of Cdc123(1-291). Diploid yeast cells heterozygote for a C-terminal HA3-fusion of either wild-type *CDC123* (upper panel; W14233) or C-terminal truncation mutant *CDC123*(1-291) (lower panel; W2880) were sporulated and subjected to tetrad dissection.

The C-terminal truncation of Cdc123 had no effect on the interaction of Cdc123 with eIF2γ, but disrupted the biological function of Cdc123.

## Supplemental Table

| | Full-length cdc123[a] | Full-length cdc123 [a] | Full-length cdc123 Se-met |
|---|---|---|---|
| **Data collection** | | | |
| Crystallization Conditions | 22.5% PEG3350 20mM $(NH_4)_2C_4H_4O_6$ +ATP-$Mg^{2+}$ | 22.5% PEG3350 20mM$(NH_4)_2C_4H_4O_6$ | 20%PEG3350 0.1M $NH_4F$ |
| Space group | $P2_12_12_1$ | C222 | C222 |
| Cell dimensions | | | |
| *a*, *b*, *c* (Å) | 87.69 100.19 129.68 | 87.17 208.07 87.45 | 86.42 295.6 86.00 |
| *a*, *b*, $\gamma$ (°) | 90 90 90 | 90 90 90 | 90 90 90 |
| Molecules in a.u | 4 | 2 | 2 |
| Resolution (Å) | 49.1-3.0 | 49.10-3.24 | 49.4-5.5 |
| $R_{sym}$ | 10.5 (135.0)[b] | 4.8 (71.1) | 7.6 (42.1) |
| $I/\sigma I$ | 13.55 (1.29) | 19.68 (2.42) | 23.01 (6.85) |
| CC1/2 | 99.9 (61.2) | 99.9 (81.3) | 99.9 (97.3) |
| Completeness (%) | 99.9 (99.8) | 96.8 (95.9) | 99.8 (100) |
| Redundancy | 7.3 (7.4) | 5.51 (5.50) | 14.36 (14.88) |
| | | | |
| sigAno | | | 1.671 (0.943) |
| Ano. Correlation (%) | | | 57 (23) |

**Table S1:** Data collection statistics for Sp-cdc123 structure resolution

[a]A single crystal was used for data collection.

[b]Values in parentheses are for highest-resolution shell.

## Supplemental Experimental Procedures

### Protein expression and purification

*Sc-γDIII*

Sc-γDIII domain was purified from 1 liter of culture of BL21 Rosetta *E. coli* cells transformed with pET3a-Sc-γDIII. The pellet was resuspended in buffer A. After sonication and centrifugation, the extract was loaded onto an S-Sepharose column (16mm x 20cm; GE-Healthcare) equilibrated in buffer A. A gradient from 200 mM NaCl to 1 M NaCl was used for elution (300 mL at a flow rate of 2.5

mL/min). The recovered fractions were pooled, concentrated and loaded onto a Superdex 200 HR 10/30 column equilibrated in buffer A. The purified protein was concentrated to 10 mg/mL.

An N-terminally tagged version of Sc-γDIII domain was purified from BL21 Rosetta *E. coli* cells transformed with PWS3915 and induced with 0.2% rhamnose after overnight culture at 37°C. The same purification protocol as the one described above was used for the purification except that a first step of affinity chromatography was added. The resulting protein was used to perform titration experiments using isothermal calorimetry (ITC).

*Sc-Cdc123*

Plasmid pWS1389 allows expression of an N-terminally his-tagged version of Sc-Cdc123. The plasmid was transformed into BL21 Rosetta *E. coli* cells. Overexpression of Sc-Cdc123 was induced with 0.2% rhamnose after overnight culture at 37°C. After induction, the culture was continued for 4 hours at 18°C. The cells were resuspended in buffer B. After sonication and centrifugation, the crude extract was loaded onto a column (4 mL) containing Talon affinity resin (Clontech) equilibrated in buffer B. Sc-Cdc123 was eluted with buffer B containing 125 mM imidazole. After dialysis against buffer C (10 mM HEPES pH 7.5, 100 mM NaCl, 3 mM 2-mercaptoethanol, 0.1 mM PMSF, 0.1 mM benzamidine), the protein was loaded onto a Q-Sepharose column (0.8 mm x 3 cm; GE-Healthcare) equilibrated in buffer C. A gradient from 100 mM NaCl to 600 mM NaCl was used for elution (60 mL at a flow rate of 2mL/min). The recovered protein was finally concentrated and loaded onto a Superdex 200 column (HR 10/30; GE Healthcare) equilibrated in buffer A. Fractions containing Sp-Cdc123:Sc-γDIII were pooled and concentrated to 10 mg/mL.

**SAXS data collection**

SAXS experiments were conducted on beamline SWING at the SOLEIL Synchrotron ($\lambda$ = 1.033 Å). The Aviex charge-coupled device detector was positioned at a distance of 2076 mm from the sample, with the direct beam off-centered. Data were collected in the $Q$-range 0.008–0.5 $Å^{-1}$ ($Q = 4\pi\sin\theta/\lambda$, $2\theta$ is the scattering angle). All solutions were circulated in a thermostated (15 °C) quartz

capillary with a diameter of 1.5 mm and a wall thickness of 10 µm, positioned within a vacuum chamber.

For data collection purified complex Sp-Cdc123-γDIII (*c.a* 20 nanomoles in 100-200 µl) was injected on a size-exclusion column (Agilent© BioSEC 3-300) using an Agilent© High Performance Liquid Chromatography system and eluted directly into the SAXS flow-through capillary cell at a flow rate of 0.2 mL/min. The elution buffer was 10 mM Hepes pH 7.5, 500 mM NaCl. SAXS data were collected online, with a frame duration of 1.5 s and a dead time between frames of 1.0 s. A large number of frames were collected during the first minutes of the elution and averaged to account for buffer scattering, which was subsequently subtracted from the signal during elution of the protein complex. Selected curves corresponding to the main elution peak were averaged on the basis of identical shapes (David and Perez, 2009). Data reduction to absolute units, frame averaging and subtraction, were performed using FOXTROT (http://www.synchrotron-soleil.fr/Recherche/LignesLumiere/SWING). All subsequent data processing, analysis, and modeling steps were carried out with PRIMUS and other programs of the ATSAS suite (Konarev et al., 2006). Scattered intensity curves were calculated from the atomic coordinates of the crystallographic structures using CRYSOL (Svergun et al., 1995) with 50 harmonics. This program was also used to fit the calculated curve to the experimental one, by adjusting the excluded volume, the averaged atomic radius and the contrast of the hydratation layer surrounding the particle in solution.

**Pull-Down assays**

A 15 mL culture of wt-Sc-γDIII or mutant Sc-γDIII (E460A, R504A, W509A) was mixed to a 15 mL culture of N-terminally tagged version of Sp-Cdc123, centrifugated and resuspended in 1 mL of buffer B. After sonication, the insoluble fraction was removed by centrifugation. The crude extract was then mixed with 200 µL of metal affinity resin (Talon, Clontech) to perform batch purification. After several rounds of beads washing, the retained complex was eluted from the resin with buffer B supplemented with 125 mM imidazole. A fixed volume aliquot of each step of the batch purification was loaded onto a 12% polyacrylamide SDS gel (Figure S4).

## ITC

*Binding of γDIII*

Before ITC measurements, proteins were dialyzed against buffer B. Titrations curves were obtained using a MicroCal200 apparatus (Malvern). Sc-Cdc123 (250 µL, 20 µM) was titrated by 20 injections (4 µL) of Sc-γDIII at a concentration of 150 µM. A typical titration curve is shown in Figure S3C. The deduced dissociation constant for the Sc-γDIII:Sc-Cdc123 complex was 2.5 ± 0.5 µM.

*Binding of ATP*

Before ITC measurements proteins were dialyzed against buffer A supplemented with 5 mM $MgCl_2$. Titrations curves were obtained using a MicroCal200 apparatus (Malvern). 250 µL of Sp-Cdc123 or of Sp-Cdc123-γDIII complex, (125 µM) was titrated by 20 injections (4 µL) of ATP at a concentration of 1.25 mM. A typical titration curve is shown in Figure S3A. The deduced dissociation constant were similar for the Sc-Cdc123:ATP-$Mg^{2+}$ complex (67 ± 13 µM) and for the Sc-Cdc123-γDIII:ATP-$Mg^{2+}$ complex (57 ± 7 µM). Reported results are mean ± s.d. from at least two independent experiments.

## Yeast methods

For growth, transformation, mating, sporulation, and tetrad dissection of budding yeast cells, standard protocols were followed (Ausubel et al., 2005). Yeast strains used in this study are isogenic derivatives of W303 and listed below. Cells were grown in YEP complex medium containing adenine (100 mg/L), tryptophan (200 mg/L), $KH_2PO_4$ (10 mM), and glucose (2%) or raffinose (2%). To induce expression from the *GAL1* promoter, 2% galactose was added to YEP complex medium containing raffinose.

| strain | relevant genotype | figure |
|---|---|---|
| W276 | *MATα his3 trp1 ura3::lexA-op-lacZ-URA3 leu2::lexA-op-LEU2* | S9, S11 |
| W2880 | *MATa/α CDC123/CDC123(1-291)-HA3-HIS3MX6* | S11 |
| W7743 | *MATα CDC123 trp1::pTEF2-3xFLAG-GCD11-tCYC1-TRP1 ura3::pTEF2-SUI2-tCYC1-URA3* | 5B |
| W7745 | *MATα cdc123-delta::kanMX4 trp1::pTEF2-3xFLAG-GCD11-tCYC1-TRP1 ura3::pTEF2-SUI2-tCYC1-URA3* | 5B |
| W9876 | *MATa/α SUI2/SUI2-MYC13-HIS3MX6* | S10 |
| W9878 | *MATα ura3* | S11 |
| W13930 | *MATα cdc123-delta::kanMX4 trp1::pTEF2-3xFLAG-GCD11-tCYC1-TRP1 ura3::pTEF2-SUI2-tCYC1-URA3 leu2::pCDC123-CDC123-tCYC1-LEU2* | 5B |
| W13931 | *MATα cdc123-delta::kanMX4 trp1::pTEF2-3xFLAG-GCD11-tCYC1-TRP1 ura3::pTEF2-SUI2-tCYC1-URA3 leu2::pCDC123-CDC123DIN-tCYC1-LEU2* | 5B |
| W13935 | *MATa/α CDC123/cdc123-delta::kanMX4 pCDC123-CDC123D252A-tCYC1-URA3 (ARS/CEN)* | 5B |
| W13936 | *MATa/α CDC123/cdc123-delta::kanMX4 pCDC123-CDC123DIN(266-268)-tCYC1-URA3 (ARS/CEN)* | 5B |
| W14145 | *MATa/α CDC123/cdc123-delta::kanMX4 pCDC123-CDC123-tCYC1-URA3 (ARS/CEN)* | 5B |
| W14185 | *MATa/α SUI2/SUI2-MYC13-HIS3MX6 ura3/ura3::pTEF2-CDC123-FLAG3-tCYC1-URA3* | S10 |
| W14186 | *MATa/α SUI2/SUI2-MYC13-HIS3MX6 ura3/ura3::pTEF2-CDC123DIN-FLAG3-tCYC1-URA3* | S10 |
| W14233 | *MATa/α CDC123/CDC123-HA3-HIS3MX6* | S11 |
| W14236 | *MATα ura3::pGAL1-CDC123-FLAG3-tCYC1-URA3* | S11 |
| W14237 | *MATα ura3::pGAL1-CDC123(1-291)-FLAG3-tCYC1-URA3* | S11 |
| W14238 | *MATα cdc123-delta::kanMX4 trp1::pTEF2-3xFLAG-GCD11-tCYC1-TRP1 ura3::pTEF2-SUI2-tCYC1-URA3 leu2::pCDC123-CDC123D252A-tCYC1-LEU2* | 5B |

Yeast strains

**DNA constructs and genetic manipulation**

Yeast plasmid constructs used in this study are derivatives of pRS vectors (Sikorski and Hieter, 1989), pEG202 or pJG4-5 (Ausubel et al., 2005) and are listed below. C-terminal epitope fusions of endogenous genes and the C-terminal truncation of *CDC123* (*CDC123*(1-291)) were constructed by PCR-based epitope tagging (Longtine et al., 1998). Site-directed mutagenesis (Quick-change; Stratagene) was used to replace the D266, I267, N268, and D252 codons of *CDC123* by alanine codons.

| name | description | vector | figure |
|---|---|---|---|
| pED002 | *pGAL-NLS-AD-HA-GCD11-delta L1 loop(delta325-331)* | pJG4-5 | S9 |
| pJG4-5 | *pGAL-NLS-AD-HA-MCS, TRP1, 2µ* | | S9, S11 |
| pWS1378 | *pCDC123-CDC123-tCYC1, ARS/CEN* | pRS416 | 5B |
| pWS1463 | *pADH-lexA-CDC123* | pEG202 | S9, S11 |
| pWS1513 | *pGAL-NLS-AD-HA-GCD11* | pJG4-5 | S9, S11 |
| pWS1535 | *pADH-lexA-SUI3* | pEG202 | S9 |
| pWS1537 | *pADH-lexA-SUI2* | pEG202 | S9 |
| pWS1846 | *pCDC123-CDC123-tCYC1* | pRS305 | 5B |
| pWS3801 | *pADH-lexA-CDC123(1-291)* | pEG202 | S11 |
| pWS4398 | *pCDC123-CDC123D252A-tCYC1, ARS/CEN* | pRS416 | 5B |
| pWS4399 | *pCDC123-CDC123D266A/I267A/N268A-tCYC1, ARS/CEN* | pRS416 | 5B |
| pWS4465 | *pCDC123-CDC123D266A/I267A/N268A-tCYC1* | pRS305 | 5B |
| pWS4488 | *pTEF2-CDC123-FLAG3-tCYC1* | pRS306 | S10 |
| pWS4501 | *pTEF2-CDC123D266A/I267A/N268A -FLAG3-tCYC1* | pRS306 | S10 |
| pWS4671 | *pCDC123-CDC123D252A-tCYC1* | pRS305 | 5B |
| pWS4677 | *pGAL1-CDC123-FLAG3-tCYC1* | pRS306 | S11 |
| pWS4678 | *pGAL1-CDC123(1-291)-FLAG3-tCYC1* | pRS306 | S11 |

Yeast plasmids

**Yeast-Two-Hybrid assay**

The Y2H reporter strain W276 was co-transformated with pEG202 and pJG4-5 derivatives. Transformants were spotted on synthetic complete solid medium lacking histidine and tryptophan and containing saccharose (1%) and galactose (2%). Plates were incubated over night at 30°C. β-galactosidase activity was visualized by overlaying the yeast colonies with an X-gal top agar containing sodium phosphate buffer (0.5 M, pH 7.0), DMFA (6%), X-Gal (0.2 mg/ml), SDS (0.1%), and Bacto agar (0.5%). Coloration was documented after incubation over night at 30°C.

**Yeast cell extracts, immunoprecipitation and Western analysis**

Whole cell protein extracts and immunoprecipitations were made as described (Arnold et al., 2015; Perzlmaier et al., 2013). SDS-PAGE and Western analysis were done essentially as described (Schwab et al., 2001). Mouse monoclonal antibodies M2 (Sigma-Aldrich) and 9E10 were used for detection of FLAG-tagged and MYC-tagged proteins, respectively. eIF2α (Sui2), eIF2γ (Gcd11), and Cdc123 were detected using a polyclonal rabbit antiserum (Sui2) or affinity-purified polyclonal rabbit antisera (Gcd11, Cdc123) (Perzlmaier et al., 2013). Detection of immunoblots was done using IRDye secondary antibodies and an Odyssey infrared imaging system (LI-COR Biosciences).

## Supplemental references


Ausubel FM, Brent R, Kingston RE, Moore DD, Seidman JG, Smith JA, Struhl K (2005) *Current Protocols in Molecular Biology*: John Wiley & Sons, Inc.

Arnold, L., Hockner, S., and Seufert, W. (2015). Insights into the cellular mechanism of the yeast ubiquitin ligase APC/C-Cdh1 from the analysis of in vivo degrons. Mol Biol Cell *26*, 843-858.

Ausubel, F.M., Brent, R., Kingston, R.E., Moore, D.D., Seidman, J.G., Smith, J.A., and Struhl, K. (2005). Current Protocols in Molecular Biology (John Wiley & Sons, Inc.).

David, G., and Perez, J. (2009). combined sampler robot and high-performance liquid chromatography: a fully automated system for biological small-angle X-ray scattering experiments at the Synchrotron SOLEIL SWING beamline. J Appl Crystallogr *42*, 892-900.

Gouet, P., Courcelle, E., Stuart, D.I., and Metoz, F. (1999). ESPript: analysis of multiple sequence alignments in PostScript. Bioinformatics *15*, 305-308.

Konarev, P.V., Volkov, V.V., Petoukhov, M.V., and Svergun, D.I. (2006). ATSAS 2.1, a program package for small-angle scattering data analysis. J Appl Crystallogr *39*, 277-286.

Larkin, M., Blackshields, G., Brown, N., Chenna, R., McGettigan, P., McWilliam, H., Valentin, F., Wallace, I., Wilm, A., Lopez, R.*, et al.* (2007). ClustalW and ClustalX version 2 Bioinformatics *23*, 2947-2948.

Longtine, M.S., McKenzie, A., 3rd, Demarini, D.J., Shah, N.G., Wach, A., Brachat, A., Philippsen, P., and Pringle, J.R. (1998). Additional modules for versatile and economical PCR-based gene deletion and modification in Saccharomyces cerevisiae. Yeast *14*, 953-961.

Miles, B.W., Thoden, J.B., Holden, H.M., and Raushel, F.M. (2002). Inactivation of the amidotransferase activity of carbamoyl phosphate synthetase by the antibiotic acivicin. J Biol Chem *277*, 4368-4373.

Miller, G.J., Wilson, M.P., Majerus, P.W., and Hurley, J.H. (2005). Specificity determinants in inositol polyphosphate synthesis: crystal structure of inositol 1,3,4-trisphosphate 5/6-kinase. Mol Cell *18*, 201-212.

Ouchi, T., Tomita, T., Horie, A., Yoshida, A., Takahashi, K., Nishida, H., Lassak, K., Taka, H., Mineki, R., Fujimura, T.*, et al.* (2013). Lysine and arginine biosyntheses mediated by a common carrier protein in Sulfolobus. Nature chemical biology *9*, 277-283.

Perzlmaier, A.F., Richter, F., and Seufert, W. (2013). Translation initiation requires cell division cycle 123 (Cdc123) to facilitate biogenesis of the eukaryotic initiation factor 2 (eIF2). J Biol Chem *288*, 21537-21546.

Roper, D.I., Huyton, T., Vagin, A., and Dodson, G. (2000). The molecular basis of vancomycin resistance in clinically relevant Enterococci: crystal structure of D-alanyl-D-lactate ligase (VanA). Proc Natl Acad Sci U S A *97*, 8921-8925.

Schwab, M., Neutzner, M., Mocker, D., and Seufert, W. (2001). Yeast Hct1 recognizes the mitotic cyclin Clb2 and other substrates of the ubiquitin ligase APC. EMBO J *20*, 5165-5175.

Sikorski, R.S., and Hieter, P. (1989). A system of shuttle vectors and yeast host strains designed for efficient manipulation of DNA in Saccharomyces cerevisiae. Genetics *122*, 19-27.

Svergun, D.I., Barberato, C., and Koch, M.H.J. (1995). CRYSOL- aprogram to evaluate X-ray solution scaterring of biological macromoleucles from atomic coordinates. J Appl Crystallogr *28*, 768-773.

Thoden, J.B., Firestine, S., Nixon, A., Benkovic, S.J., and Holden, H.M. (2000). Molecular structure of Escherichia coli PurT-encoded glycinamide ribonucleotide transformylase. Biochemistry *39*, 8791-8802.

Waterhouse, A., Procter, J., Martin, D., Clamp, M., and Barton, G. (2009). Jalview Version 2-a multiple sequence alignment editor and analysis workbench. Bioinformatics *25*, 1189-1191.

Yatime, L., Mechulam, Y., Blanquet, S., and Schmitt, E. (2006). Structural switch of the gamma subunit in an archaeal aIF2 alpha gamma heterodimer. Structure *14*, 119-128.

Zhao, G., Jin, Z., Wang, Y., Allewell, N.M., Tuchman, M., and Shi, D. (2013). Structure and function of Escherichia coli RimK, an ATP-grasp fold, L-glutamyl ligase enzyme. Proteins *81*, 1847-1854